RESEARCH ARTICLE

Unravelling controls on multi-source-to-sink systems: A stratigraphic forward model of the early–middle Cenozoic of the SW Barents Sea

Amando P. E. Lasabuda[1,2,3,4] | Domenico Chiarella[2] | Tor O. Sømme[5] | Sten-Andreas Grundvåg[1] | Anthony G. Doré[6] | Grandika Primadani[7] | Tom Arne Rydningen[1] | Jan Sverre Laberg[1] | Alfred Hanssen[1]

[1]Department of Geosciences, UiT The Arctic University of Norway, Tromsø, Norway

[2]Clastic Sedimentology Investigation (CSI), Department of Earth Sciences, Royal Holloway University of London, Egham, UK

[3]Centre for Planetary Habitability (PHAB), Department of Geosciences, University of Oslo, Oslo, Norway

[4]EarthByte Group, School of Geosciences, The University of Sydney, Sydney, New South Wales, Australia

[5]Equinor ASA, Fornebu, Norway

[6]Energy and Geoscience Institute (EGI), University of Utah, Salt Lake City, USA

[7]BeicipFranlabAsia, Kuala Lumpur, Malaysia

Correspondence
Amando P. E. Lasabuda, Department of Geosciences, University of Oslo, Oslo, Norway.
Email: amando.lasabuda@geo.uio.no

Abstract

Source-to-sink dynamics are subjected to complex interactions between erosion, sediment transfer and deposition, particularly in an evolving tectonic and climatic setting. Here we use stratigraphic forward modelling (SFM) to predict the basin-fill architecture of a multi-source-to-sink system based on a state-of-the-art numerical approach. The modelling processes consider key source-to-sink parameters such as water discharge, sediment load and grain size to simulate various sedimentary processes and transport mechanisms reflecting the dynamic interplay between erosion in the catchment area, subsidence, deposition and filling of the basin. The Cenozoic succession along the SW Barents Shelf margin provides a key area to examine controls on source-to-sink systems along a transform margin that developed during the opening of the North Atlantic when Greenland and Eurasian plates were separated (ca. 55 Ma onwards). Moreover, the gradual cooling which culminated in major glaciations in the northern hemisphere during the Quaternary (ca. 2.7 Ma), has affected the spatio-temporal evolution of the sediment routing along the western Barents Shelf margin. This study aims to characterize the relative importance of different source areas within the source-to-sink framework through SFM. In the early Eocene, the SW Barents Shelf experienced a relatively equal sediment delivery from three principal source areas: (i) Greenland to the north, (ii) the Stappen High to the east, representing a local source terrain, and (iii) a major southern source (Fennoscandia). In the middle Eocene, our best-fit modelling scenario suggests that the northern and the local eastern sources dominated over the southern source, collectively supplying large amounts of sand into the basin as evidenced by the submarine fans in Sørvestsnaget Basin. In the Oligocene (ca. 33 Ma) and Miocene (ca. 23 Ma), significant amounts of sediments were sourced from the east due to shelf-wide uplift. Finally, this study highlights the dynamic nature and controls of sediment

transfer in multi-source-to-sink systems and demonstrates the potential of SFM to unravel tectonic and climatic signals in the stratigraphic record.

KEYWORDS

Barents Sea, climate, source-to-sink, stratigraphic forward modelling, tectonics

1 | INTRODUCTION

The source-to-sink analysis investigates the link between sediment production and transport in source areas and deposition in the basin, commonly referred to as the sink (e.g. Amorosi et al., 2022; Helland-Hansen et al., 2016; Nyberg et al., 2018; Sømme, Martinsen, & Thurmond, 2009). However, when multiple source areas co-exist and are located on or near a tectonically active plate margin, changes in sediment supply driven by tectonic or geomorphic changes in the hinterland may vary significantly in time and space (e.g., Eide et al., 2017; Grundvåg et al., 2017; Hawie et al., 2017; Lasabuda, Laberg, Knutsen, & Safronova, 2018). This particularly holds true for transform margins, where source areas may move laterally to the sink. As such, the relative contribution from various source areas to the overall rate of sediment supply to basins on transform margins can be challenging to quantify, particularly in areas with limited data.

The SW Barents Sea (Figure 1a,b) is a key area to address these research problems because (1) its Cenozoic history is related to plate breakup and separation, regional uplift and erosion, subsidence and deposition, as well as sediment contributions from multiple source areas (Baig et al., 2016; Doré et al., 2016; Faleide et al., 2008; Ktenas et al., 2017; Lasabuda et al., 2021; Nyland et al., 1992; Riis & Fjeldskaar, 1992; Vorren et al., 1991); (2) it is an area with multiple sediment sources (Blaich et al., 2017; Flowerdew et al., 2023; Lasabuda, Laberg, Knutsen, & Høgseth, 2018; Smelror et al., 2009), the relative contribution of which we wish to examine; and (3) it has relatively good coverage of seismic and well data due to subsurface exploration (Henriksen, Ryseth, et al., 2011; Jakobsson, 2018; Johansen et al., 1993).

The stratigraphic forward modelling (SFM) technique is a robust tool to simulate sediment transfer and deposition in basin filling using constrained parameters (e.g. Burgess et al., 2006; Sømme, Helland-Hansen, & Granjeon, 2009). This technique has proven to be useful in predicting lateral variations and temporal evolution of sedimentary strata, particularly on 100's km scale continental margins with few seismic lines and limited tie points (e.g. Barabasch et al., 2019; Hawie et al., 2017). The modelling processes consider key source-to-sink parameters such as water discharge, sediment load and grain size reflecting the dynamic interplay between erosion in

Highlights

- For the first time, the early to middle Cenozoic multi-source-to-sink systems in the SW Barents Sea are numerically modelled using stratigraphic forward modelling (SFM).
- We investigate controls on multi-source-to-sink systems in a tectonically active plate margin with dynamic climate history.
- Results show that the multi-sources scenario is consistent with seismic and well data.
- The study demonstrates the potential of SFM to unravel tectonic and climatic signals.

the catchment area, subsidence, deposition and filling of the basin (Granjeon & Joseph, 1999; Hawie et al., 2018).

Here we present results from an SFM case study of Eocene–Miocene-aged multi-source-to-sink systems of the SW Barents Sea, Norwegian Arctic. The specific aims of the study are to (i) quantify the relative contribution of multiple source areas to the basin fill, and (ii) reveal the dominant controlling parameters and uncertainties in sediment erosion-transport-deposition in a dynamic tectonic and climatic setting. These aims will be achieved by producing best-fit models that largely match with available seismic and well data. However, we did not attempt to precisely recreate the entire SW Barents Shelf margin, but rather to use a smaller part of the system for realistic comparison of different source-to-sink parameters and to capture the relative input from different source areas.

2 | GEOLOGICAL SETTING

At the Paleocene–Eocene transition (ca. 55 Ma), the Eurasian and Greenland plates broke up and seafloor spreading occurred in the Norwegian and Greenland seas (Figure 2) (Faleide et al., 2008; Talwani & Eldholm, 1977). Along the western Barents Shelf, much of the movements related to the opening occurred along the regional transform De Geer Zone, which comprises the Hornsund Fault Zone to the north and the Senja Fracture Zone to the south. Transpressional tectonics along the northern segment of the transform, commonly
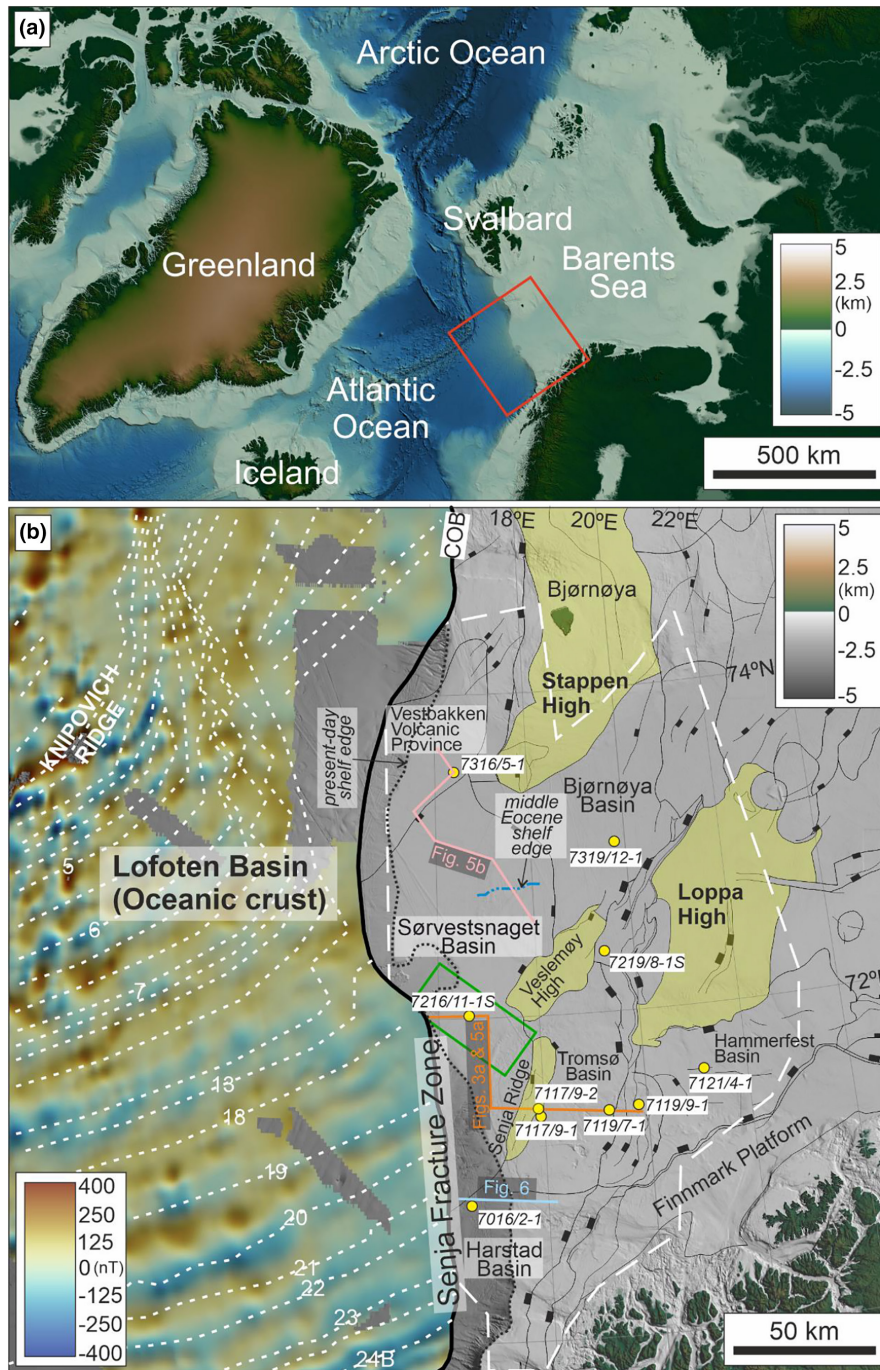
FIGURE 1 The SW Barents Sea is located in the Norwegian Arctic. (a) The location of the study area is shown by a red rectangle. Bathymetric and topographic data are derived from GEBCO (2022). (b) Structural highs are shaded with yellow. The extent of 2D seismic data is shown as long-dashed lines and the 3D seismic location is shown as green rectangle. Representative seismic profiles are shown as orange, pink and light blue lines (Figures 3a, 5a,b and 6). Wells are shown as yellow circles. The location of the middle Eocene shelf edge follows Safronova et al. (2014). Structural elements are taken from the Norwegian Offshore Directorate. Magnetic anomalies are numbered and shown as white dotted lines (Dumais et al., 2022; Gaina et al., 2017). COB, continental-ocean boundary.

attributed to the Eurekan deformation, promoted the formation of a fold-and-thrust belt along western Spitsbergen, as well as creating high topography (anticlines and domes) in the northern Barents Sea (Bergh et al., 1997; Gac et al., 2020; Piepjohn et al., 2016). Transtensional forces dominated the southern segment of the transform, resulting in the

development of a pull-apart basin and associated volcanism in the Vestbakken Volcanic Province (Faleide et al., 1988). Likewise, in the Sørvestsnaget Basin, a deep basin developed in the vicinity of the Senja Fracture Zone (Kristensen et al., 2018; Ryseth et al., 2003). Deep marine conditions prevailed in the greater parts of the SW Barents Sea for most of the
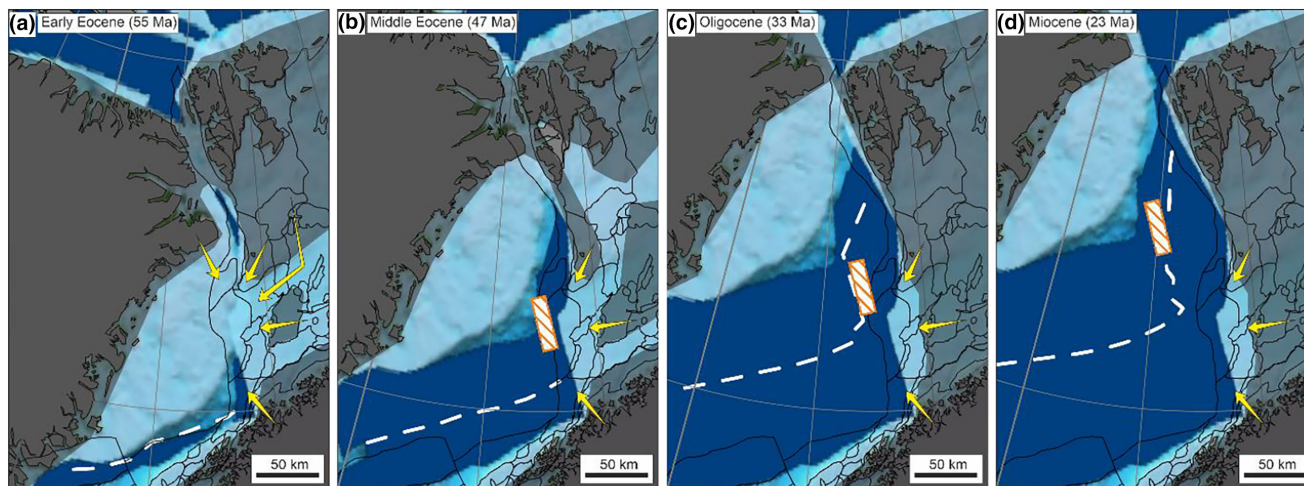
FIGURE 2 Plate tectonic reconstructions from the (a) earliest Eocene (55 Ma), (b) middle Eocene (47 Ma), (c) Oligocene (33 Ma) to (d) Miocene (23 Ma) and the interpreted sediment supply directions as shown as yellow arrows (Lasabuda, Laberg, Knutsen, & Høgseth, 2018; Lasabuda, Laberg, Knutsen, & Safronova, 2018; Smelror et al., 2009). The dark-hatched areas represent areas of erosion/non-deposition. The light and dark blue colours represent shallow and deep marine conditions. Dashed lines are the location of the mid-oceanic ridge. The orange-dashed rectangle is the approximate location of the East Greenland Ridge (Doré et al., 2016; Faleide et al., 2015). Plate tectonic configurations are reconstructed using GPlates v. 2.3 (Müller et al., 2019).

period, except on the paleo-highs (e.g. Senja Ridge, Veslemøy High) (Lasabuda et al., 2023).

In the middle Eocene (ca. 47 Ma), progradational wedges were built westward into the Sørvestsnaget Basin from the Stappen High (Lasabuda, Laberg, Knutsen, & Høgseth, 2018; Safronova et al., 2014). These shelf-edge clinoforms (e.g. Patruno et al., 2015; Patruno & Helland-Hansen, 2018; Pellegrini et al., 2020) associated with high sediment supply during this regressive phase seem to have transferred significant amounts of sediment to the deeper part of the basin where submarine fans have been interpreted from seismic and well data (Ryseth et al., 2003; Safronova et al., 2012). Some smaller clinoforms have also been observed in seismic data, prograding westward towards the Tromsø Basin suggesting a considerable sediment source area to the east (Lasabuda, Laberg, Knutsen, & Høgseth, 2018; Vorren et al., 1991).

In the Oligocene (ca. 33 Ma), major plate reorganisation took place when Greenland, being part of the North American plate, drifted towards the NW relative to the Barents Shelf and the Eurasian plate (Faleide et al., 2015). Shelf-wide uplift in the Oligocene has been attributed to mantle process (Lasabuda et al., 2021; Vågnes & Amundsen, 1993). Previous investigations indicate that shallow marine conditions prevailed in the western basins while fluvial and coastal plain to deltaic conditions characterized in the transition towards the eastern parts (Lasabuda, Laberg, Knutsen, & Høgseth, 2018; Smelror et al., 2009).

In the Miocene (ca. 23 Ma), the middle, eastern and northern parts of the Barents Shelf were still subjected to uplift and erosion. Most of the sediments were transported to the western basins by fluvial and coastal processes (Lasabuda,

Laberg, Knutsen, & Høgseth, 2018). Later (ca. 17 Ma), these sediments were reworked by ocean currents due to the opening of the Fram Strait in the late early Miocene, which allowed ocean circulation between the Atlantic and Arctic oceans. Major sediment drifts are observed along the western margin of the Barents Shelf, including the Bjørnøyrenna Drift (Jakobsson et al., 2007; Rydningen et al., 2020).

Since the Quaternary (ca. 2.7 Ma), major ice sheets developed due to the cooling of the northern hemisphere and occupied the entire Barents Shelf with several advances and retreats (Knies et al., 2009; Lasabuda, Geissler, et al., 2018; Patton et al., 2022). The Barents Sea Ice Sheet triggered subsidence of the shelf and caused subglacial erosion delivering sediments to the west (Laberg et al., 2012; Lasabuda et al., 2021; Richardsen et al., 1991). Subsequently, when the ice retreated during the deglaciation, glacial uplift occurred due to isostatic rebound that created differential paleotopographic highs (Fjeldskaar & Amantov, 2018; Patton et al., 2022). The Quaternary glaciations have also created a tilt of the sedimentary strata that may cause the loss of hydrocarbon accumulation (Ktenas et al., 2023; Løtveit et al., 2019) and change of seabed pressure which affected gas hydrate distribution (Plaza-Faverola et al., 2022).

3 | DATA AND METHODOLOGY

3.1 | Seismic and well data

We have interpreted five key seismic horizons, here referred to as the Base Eocene (ca. 55 Ma), Base middle Eocene
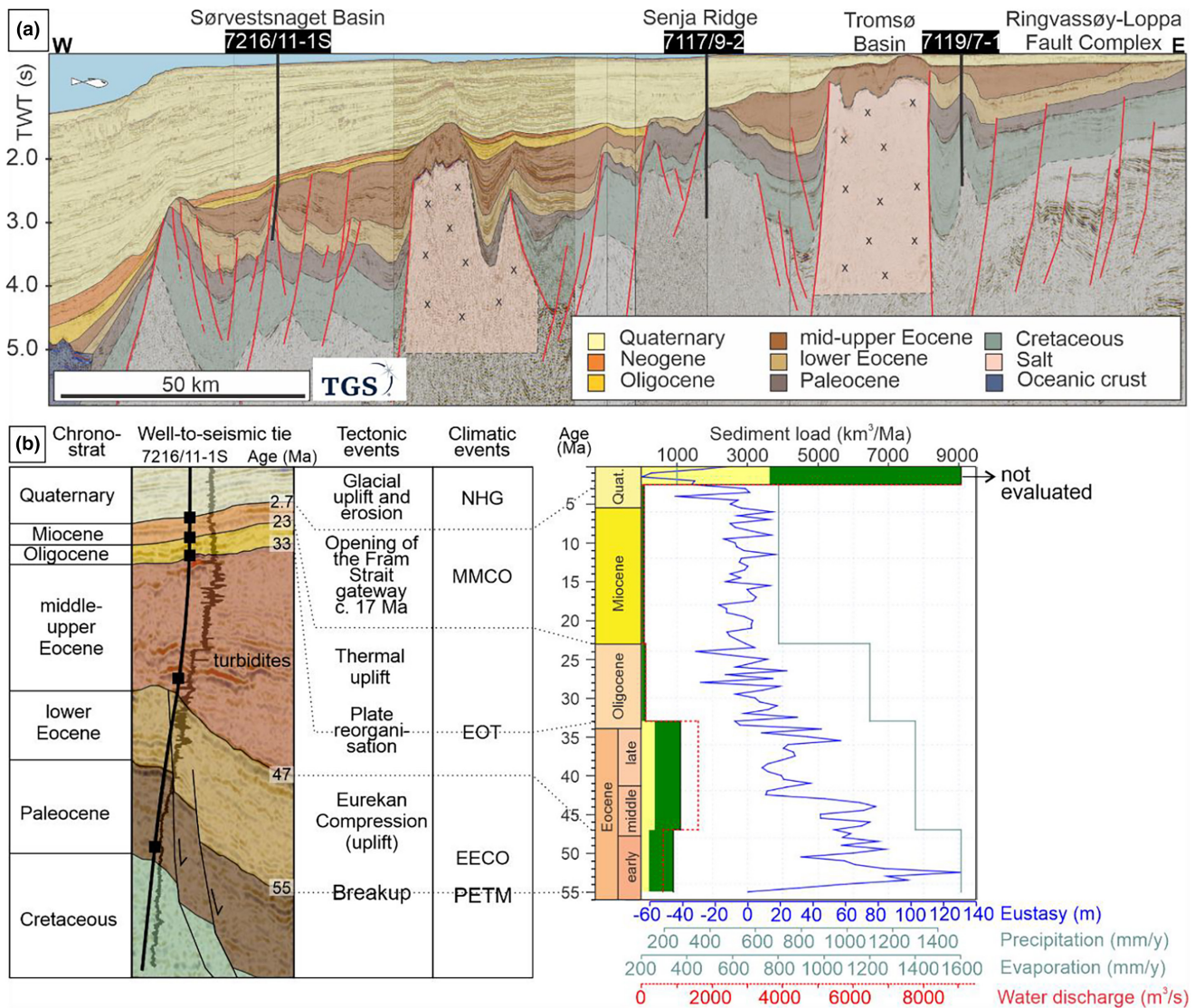
FIGURE 3 (a) Regional E–W-oriented seismic transect of the SW Barents Sea adapted from Lasabuda, Laberg, Knutsen, and Høgseth (2018). (b) Well-to-seismic tie to well 7216/11-1S including the chronostratigraphy, age, paleoenvironment, tectonic and climatic events (Kristensen et al., 2018; Lasabuda, Laberg, Knutsen, & Høgseth, 2018). Eustatic sea-level curve according to Miller et al. (2005). Total water discharge and sediment supply computed in this study are shown together with the proportion of sandstone and shale represented by yellow and green bars. Rainfall and evaporation estimates are based on Samuels and Hopkins (2017). EECO, Early Eocene Climate Optimum; EOT, Eocene–Oligocene Transition; MMCO, Middle Miocene Climate Optimum; NHG, Northern Hemisphere Glaciations; PETM, Paleocene–Eocene Thermal Maximum. For the location of the seismic profile, see Figure 1b.

(ca. 47 Ma), Base Oligocene (ca. 33 Ma), Base Miocene (ca. 23 Ma) and Base Quaternary (ca. 2.7 Ma), thus conforming to Lasabuda, Laberg, Knutsen, and Høgseth (2018). The interpretation was based on 2D-3D seismic data and tied to well data (Figure 3). The vertical seismic resolution is about 26 m considering the P-wave velocity and the frequency is approximately 2100 m/s and 20 Hz on the targeted Eocene interval in the 3D seismic cube NH-9803 (Safronova et al., 2014). The surface sizes are varied from $119.6 \times 10^3 \, km^2$ for the Eocene surface to $171.6 \times 10^3 \, km^2$ for the Miocene surface (Lasabuda, Laberg, Knutsen, & Høgseth, 2018). The Two-Way-Time (TWT) surfaces were

converted to depth using the J-Cube velocity model by TGS. The depth-converted surfaces were utilised as input for the reconstruction of the paleobathymetry and paleotopography of the study area (see below).

Five wells (i.e. 7316/5-1, 7216/11-1S, 7117/9-1, 7117/9-2, 7016/2-1) were used as a basis for lithological input (i.e. composition and ratio of sandstone and shale) for the simulation and to calibrate the modelling results (Figures 3b and 4a). The chronology of the Cenozoic succession follows well tops from the Norwegian Offshore Directorate. For the Oligocene and Miocene strata, we refer to biostratigraphy analysis by Eidvin et al. (1993, 2022).

3.2 | Stratigraphic forward modelling using DionisosFlow

We used DionisosFlow, a deterministic forward stratigraphic modelling software that simulates basin infill over geologic time scales and which has proven suitable for large-scale (100's of km) sedimentary systems (Barabasch et al., 2019; Granjeon & Joseph, 1999; Hawie et al., 2017). The key input parameters include lithological composition, estimates of sediment supply, water discharge, paleo-precipitation, as well as paleo-evaporation (Table 1). The software reproduces basin accommodation considering subsidence, uplift and sea-level fluctuations and simulates sediment transport using a diffusion equation below (e.g. Hawie et al., 2017; Sømme, Helland-Hansen, & Granjeon, 2009). The diffusion principle relies on: (i) hill-slope creeping (linear slope-driven diffusion), and (ii) water discharge-driven transport (non-linear water discharge and slope-driven diffusion) as formulated below (Tucker & Slingerland, 1994; Willgoose et al., 1991).

$$Q_s = -K_{si}/\Delta h - K_{wi}Q_w^m S^n$$

Q_s: sediment flux [km^2/year]; h [m]: elevation; K_s and K_w: diffusion coefficient, respectively, for the slow creeping transport and the faster water-driven process [km^2/year], with "i" referring to transport lithologies; Q_w: dimensionless local water discharge at the cell (normalised by 100 m^3/km^2); S: the local gradient of the basin slope; n and m: constant, usually between 1 and 2 (Tucker & Slingerland, 1994).

Below is the numerical setup used in this study including the key input for the modelling.

3.2.1 | Domain definition

We defined an area of 320×80 km with a grid size of 5×5 km (Figure 4a,b). This domain covers most parts of the Sørvestsnaget Basin and the Senja Ridge, and small parts of the Veslemøy High, the Vestbakken Volcanic Province, and the Bjørnøya Basin. Multiple wells with Cenozoic strata are also present, allowing for accurate modelling calibration (Figure 4a).

When delineating the size of the study area, we refer to the study of Flowerdew et al. (2023) who used sediment provenance analysis to define different source areas in the SW Barents Sea. To the north-northeast, it is bounded by the Stappen High to capture sediment input from the high or northern source, (i.e., Svalbard) area (Figure 2). The middle part of the eastern border represents an entry for sediment input from the Loppa High and southern Barents Shelf sources (Figure 4a). To the south, we expect sediment input predominantly from Fennoscandia. Therefore, the size and location of the study are considered large enough to capture a representative amount of the different sediment sources at different times modelled.
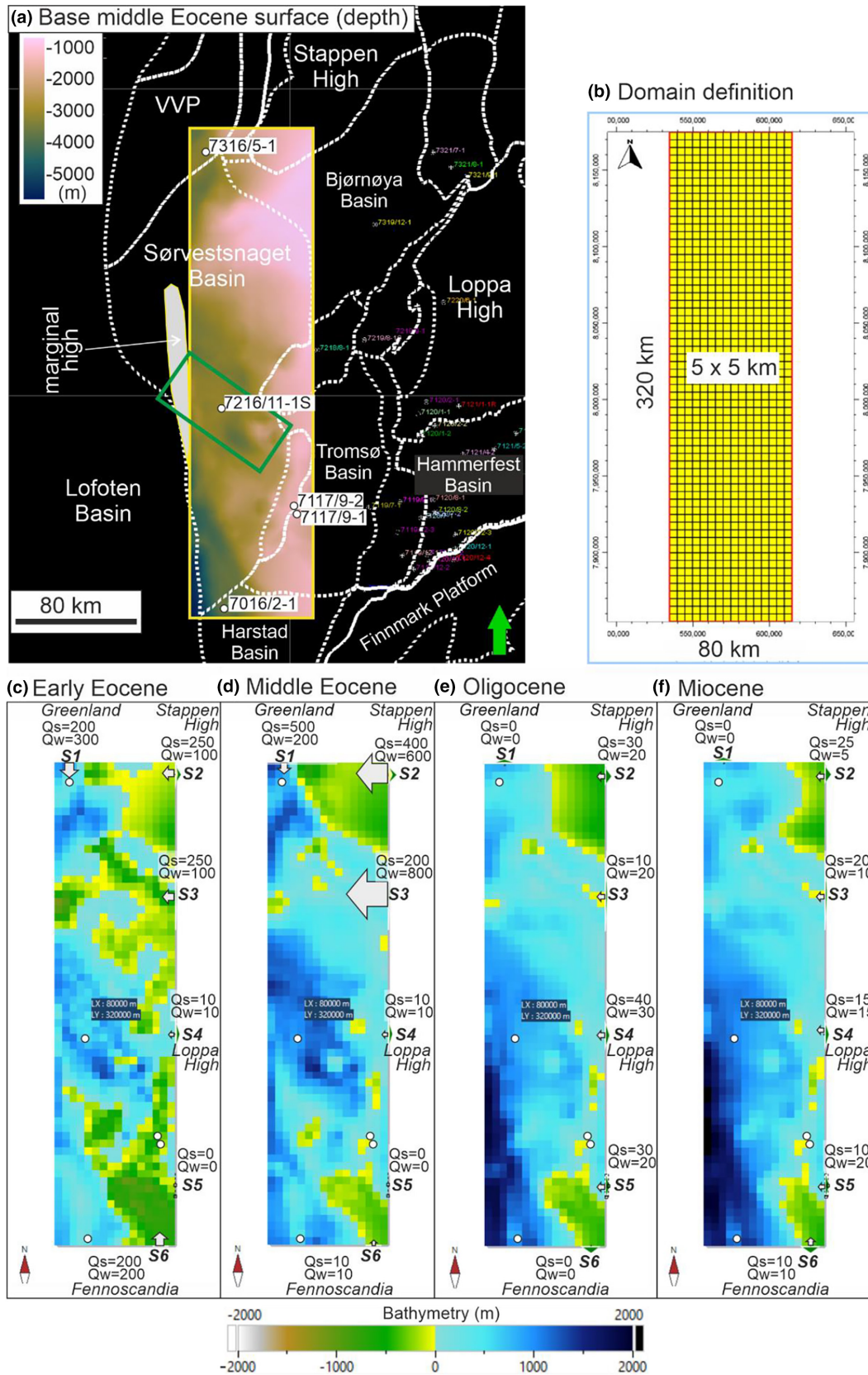
To the west-southwest, we delineate the study area following the location of the Senja Fracture Zone (Figure 1b) and the marginal high (Figure 4a; Lasabuda, Laberg, Knutsen, & Høgseth, 2018; Kristensen et al., 2018). These structural elements would largely limit the sediment deposition towards the oceanic Lofoten Basin (Figure 4a). To the west-northwest, the study area was confined by the development of the East Greenland Ridge in the Eocene (Doré et al., 2016; Faleide et al., 2015), which also likely prevented sediment deposition towards the Lofoten Basin through this sector (Figure 2b). Note that DionisosFlow can only accept rectangle shape input for the modelling. Thus, we set the western boundary to exclude the oceanic Lofoten Basin, which is beyond the scope of this work.

3.2.2 | Paleobathymetry and structural evolution

The paleobathymetric maps used in this study follow Lasabuda et al. (2023). Maps were reconstructed using backstripping analysis where each stratigraphic unit was sequentially removed and restored for the compaction effect, flexural isostasy, and thermal subsidence to produce a realistic paleobathymetry and paleotopography (see Lasabuda et al., 2023) (Figure 4c–f).

We have also applied sediment compaction using Sclater and Christie (1980)'s curve and flexural isostatic components following Lasabuda et al. (2023) such as Effective Elastic Thickness of 5 km, Poisson Ratio

FIGURE 4 The numerical setup for the domain size and sediment supply in this study. (a) Example of a depth-converted surface of the base middle Eocene generated from seismic mapping from Lasabuda et al. (2023). Five wells are used as control as shown in white circles. The location of the 3D seismic survey is shown as a green rectangle. (b) The domain size for the modelling is 320×80 km with a grid size of 5×5 km. The corresponding paleobathymetric and paleotopographic configurations following Lasabuda et al. (2023), modelled sediment input directions and lithological compositions for four different periods: (c) the early Eocene ca. 55 Ma, (d) the middle Eocene ca. 47 Ma, (e) the Oligocene ca. 33 Ma, and (f) the Miocene ca. 23 Ma. The arrows and their sizes indicate the direction and magnitude of the water discharge (Q_w). VVP, Vestbakken Volcanic Province.

(a) Base middle Eocene surface (depth)

(b) Domain definition

(c) Early Eocene **(d)** Middle Eocene **(e)** Oligocene **(f)** Miocene

Bathymetry (m)

coefficient of 0.25, Flexural Rigidity of 1.14 Nm, Flexural length of 10 km and Young Modulus of 103 Gpa to simulate the basin evolution realistically. These values are commonly applied in formerly glaciated basins, for example in the Barents Sea (e.g. Baig et al., 2016; Klausen & Helland-Hansen, 2018).

WILEY **Basin Research** IAS EAGE

TABLE 1 Key parameters used for the best-fit model in this study.

Interval	Age (Ma)	Diffusion coefficient (km³/year)		Sediment supply: Q_s (km³/Ma) and Q_w (m³/s)												Precipitation (mm/year)	Evaporation (mm/year)
		K_s	K_w	S1		S2		S3		S4		S5		S6			
				Q_s	Q_w	Q_s	Q_w	Q_s	Q_w	Q_s	Q_w	Q_s	Q_w	Q_s	Q_w		
Miocene	23	3	5	0	0	25	0	20	5	15	15	10	20	10	10	700	800
Oligocene	33	3	5	0	0	30	0	10	20	40	30	30	20	0	0	1100	1200
Mid Eocene	47	3	5	500	200	400	200	200	600	10	800	0	0	10	10	1300	1400
Early Eocene	55	3	5	200	300	250	300	250	100	10	10	0	0	200	200	1500	1600

Furthermore, we applied slope failure mode with critical slope failure of 50 m/km for mud and 100 m/km for sand to model slope instability. The basement is also considered stable (i.e. not behave as sediment) in a similar sense to an analogue laboratory modelling. For the erosion model, we defined a uniform weathering rate with maximum substratum and sediment weathering rate of 5 m/Ma to allow for local erosion from intrabasinal highs.

3.2.3 | Sediment supply: Source direction, sediment load (Q_s) and water discharge (Q_w)

Six sediment sources were defined: S1 (Greenland), S2 (Stappen High), S3 (Undifferentiated northeastern source), S4 (Loppa High), S5 (Undifferentiated southeastern source), and S6 (Fennoscandian) (Figure 4c–f). To obtain Q_w and Q_s, we adapted graphs from Hawie et al. (2017) who used a relationship between Q_w and drainage area (Dai & Trenberth, 2002) and between Q_s, drainage area, and relief (Milliman & Syvitski, 1992). The initial Q_s values presented here have been scaled down following Q_s and drainage area estimates and paleogeographical reconstructions by Lasabuda, Laberg, Knutsen, and Høgseth (2018) and Lasabuda, Laberg, Knutsen, and Safronova (2018) based on a regional mapping study and volumetric mass balance approach. We have calibrated these numbers with geological observations from other studies and key tectonic events in the region to ensure consistency (e.g. Doré et al., 2016; Faleide et al., 2015; Helland-Hansen & Grundvåg, 2021; Henriksen, Ryseth, et al., 2011; Piepjohn et al., 2016; Rydningen et al., 2020; Smelror et al., 2009).

For example, the Q_s estimates of S1 (Greenland) in the early Eocene (Figure S1) will follow the Q_s trend from a landscape that was likely to be upland to mountainous, (i.e., 600 < relief < 1200 m) (Lasabuda, Laberg, Knutsen, & Safronova, 2018) due to major Eurekan compression from Greenland to Svalbard/northern Barents Shelf (Petersen et al., 2016; Piepjohn et al., 2016). This estimated Q_s value (Figure S1b) was then plotted to obtain the water discharge value assuming the same size of drainage area occurred (Figure S1a). As long as the water discharge follows the increasing trend with the drainage area, then the chosen parameter is considered valid. Generally, the magnitude of fluvial discharge (Q_w) value (in m³/s) shows consistency when it is about the same as the Q_s value (km³/Ma) (e.g. Hawie et al., 2017, 2018; Sangster et al., 2019). The lithological compositions (i.e. sandstone-mudstone ratio) for each sediment source were computed following Lasabuda et al. (2023) based on Gamma Ray logs and Vshale analysis of well data. We excluded the simulation for the Quaternary

(after 2.7 Ma) due to the computation algorithm that was not specifically set to address glacial sediment transports and therefore the Quaternary deposit is not evaluated/discussed in this study (Figure 3b).

3.2.4 | Climate (evaporation, precipitation and eustatic sea level)

Since the software does not use temperature as an input, climatic components used in the modelling were represented by precipitation and evaporation rates (mm/year). We interpolated paleo-rates from North America by Samuels and Hopkins (2017) which are comparable to our study area due to a relatively similar latitude (Greenwood et al., 2010; Schubert et al., 2012). We have calibrated our analogue from North America (Retallack, 2007; Samuels & Hopkins, 2017) with time-specific studies and they show similarities. For example, our mean annual precipitation for Eocene input is 1100–1600 mm/year compared to the mean annual precipitation of the Eocene in Arctic Canada of 930–1900 mm/year (Greenwood et al., 2010; Schubert et al., 2012). These numbers are consistent with a moderately temperate climate with high precipitation rates in Svalbard in Paleogene times (Golovneva et al., 2023; Helland-Hansen & Grundvåg, 2021; Uhl et al., 2007). For the Oligocene, we set 1000 mm/year (Figure 3b), which is in agreement with the mean annual precipitation from Arctic Siberia (800–1200 m/year) based on Popova et al. (2012). Another calibration shows that our input of 700 mm/year for Miocene precipitation (Figure 3b) fits well with 500–1200 mm/year estimates for the late Miocene in the Arctic Siberia (Popova et al., 2012; Schubert et al., 2017). In addition, the sea-level curve used here follows that of Miller et al. (2005) (Figure 3b).

3.3 | Uncertainty

We have considered key uncertainties in this study related to paleobathymetric reconstructions and boundary conditions.

3.3.1 | Paleobathymetric reconstructions

Regional stratigraphic surfaces were created (in two-way travel time) based on 2D seismic data with an additional 3D seismic cube (Figure 1). Surfaces were then converted to depth domain using TGS velocity model in which uncertainty may be present related to velocity picking. These surfaces and their corresponding sedimentary units were backstripped, decompacted, and isostatically restored in

order to generate paleobathymetric surfaces (Lasabuda et al., 2023). Detailed steps in generating paleobathymetry surfaces and associated uncertainties (e.g. lithospheric thickness, compaction curves) have been described in Lasabuda et al. (2023).

The study area is located in a transform margin at a period where two tectonic plates slid relatively one another (Doré et al., 2016; Faleide et al., 2015; Talwani & Eldholm, 1977). There is an uncertainty related to the quantification of thermal effect that potentially influenced the paleobathymetry adjacent to the oceanic part (Lasabuda et al., 2023). We have modified and interpolated the bathymetry on the oceanic part (in the southwesternmost part of the study area) following the depth trend from adjacent continental slopes.

The Iceland plume may also play a role in the paleobathymetric reconstruction by uplifting a region due to the spherical upward-forcing pattern centred in Iceland (Jones et al., 2002; Jones & White, 2003). This plume-associated dynamic topography around NE Atlantic began as early as in the Cretaceous–Paleocene boundary and is believed to have impacted older strata within the radius of 1800 km from Iceland (Jones et al., 2014; Jones & White, 2003). However, the study area is located in a zone between 1370 and 1800 km away from Iceland where the plume effects have very little influence (Jones et al., 2014). Moreover, the plume would deflate during the Cenozoic breakup (ca. 55 Ma) evidenced by transgression along the Norwegian and UK margins in the early Eocene (Sømme et al., 2023). Therefore, this uplift mechanism would not significantly affect the paleobathymetric reconstruction in the study area (Lasabuda et al., 2023).

3.3.2 | Boundary conditions

Since the modelling domain only covers a part of the regional sink of the SW Barents Sea, we have reduced the overall sediment supply parameters. For example, the estimated value of the total Eocene sediment discharge is in the order of $Q_s = 8800$ km³/Ma or 8.8×10^6 t/y from Lasabuda, Laberg, Knutsen, and Høgseth (2018) compared to a computed value of $Q_s = 2030$ km³/Ma in this study (Table 1). Note that the sediment loads presented here do not represent the actual size of the drainage area, i.e., that is also why it differs from the Q_s values of Lasabuda, Laberg, Knutsen, and Høgseth (2018), although it will still capture the likely relief of the source area (Figures S1–S19). The Q_s values here show a best-fit estimate comprising different scenarios and configurations of sediment flux towards the sink area (Figures S20–S23). Therefore, sediment supply parameters do not represent the actual magnitude of sediment discharge and erosion in the source area. These will
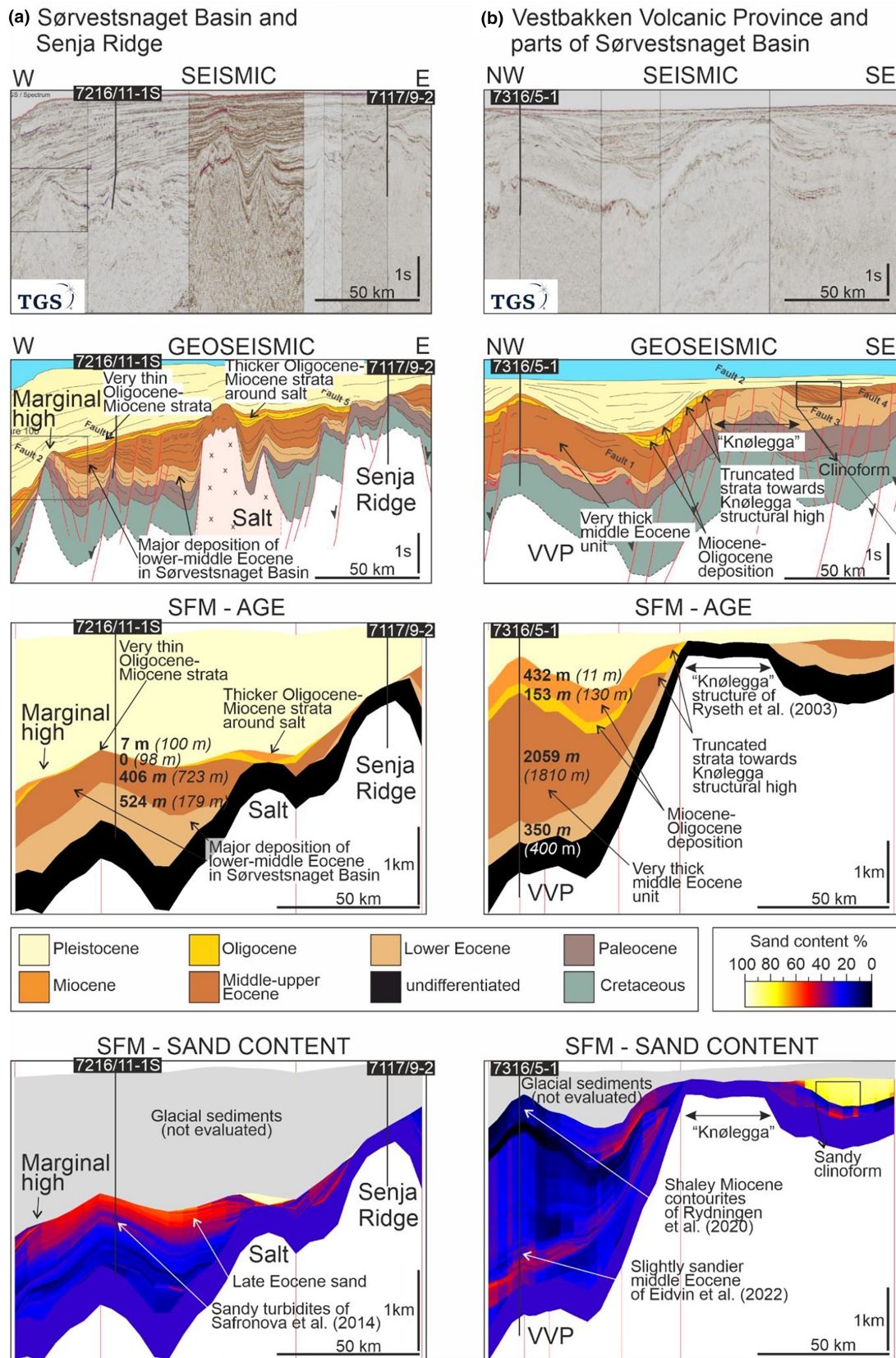
FIGURE 5 The comparison between seismic and geoseismic of Lasabuda, Laberg, Knutsen, and Høgseth (2018) and SFM result showing depositional unit and sand content (VE: 15×). At well locations, the thickness of each depositional unit (i.e. lower Eocene, middle Eocene, Oligocene and Miocene) from the model is shown in bold, while thickness based on formation well tops is shown in (*italic*). (a) The Sørvestsnaget Basin and Senja Ridge; (b) Vestbakken Volcanic Province (VVP) and parts of the Sørvestsnaget Basin. For the location of the seismic profiles, see Figure 1b.

be reflected in the local variation in thickness between modelled results and well data (e.g. Figures 5 and 6) as we are more interested in the large-scale stratigraphy and depositional trend in the basin filling.

There is also uncertainty in the sedimentary process involved in the modelling. Opening of the Fram Strait, the only deepwater gateway which allows water mass exchange between the Arctic and the Atlantic oceans, in the early Miocene introduced contour currents to the study area. Similar processes have been documented in other present-day and ancient strait settings, including the Rifian Corridor, as well as the Gibraltar and Messina straits (De Weger et al., 2021; Longhitano & Chiarella, 2020). Such currents may rework sediment from nearby sources but may also transport sediments for long distances (Stow et al., 2008). The present version of the software is not able to model this sediment transport process. However, we modified the direction of wave energy facing north to mimic a sediment transport process going northwards. We also lowered the Q_s value for the Miocene interval, i.e., from $110\,km^3$/Ma in the Oligocene to $80\,km^3$/Ma in the Miocene (Table 1) to reduce the gravity-driven effects when sediment entered the slope area.

4 | RESULTS

4.1 | Early Eocene (ca. 55–47 Ma)

The total sediment load (Q_s) was set to $910\,km^3$/Ma comprising of key supply from S1/Greenland, S2/Stappen High, S3/undifferentiated northeastern source, S4/Loppa High, and S6/Fennoscandia (Figure 4c; Figures S1–S5). The water discharge (Q_w) was set to $710\,m^3$/s for the total duration of eight million years during the early Eocene (55–47 Ma)—see Section 3.3.2 on how the sediment load has been determined and what it represents.

At the location of wells 7216/11-1S, 7316/5-1 and 7016/2-1, our model shows thicknesses of 524 m, 350 m and 47 m while the strata at these wells show thicknesses of 179, 400 and 109 m, respectively (Figures 5a,b and 6). Despite a large mismatch specifically at well 7216/11-1S (Figure 5a), we observe a similar trend of relatively thick lower Eocene interval on seismic data indicating a substantial deposition took place at the Sørvestsnaget Basin. Differential thickening in the Sørvestsnaget Basin may be related to fault and fold growth (e.g. towards the Knølegga structure of Ryseth et al. (2003) in Figure 5b). The lower Eocene interval thins in the Harstad Basin and towards bathymetric/topographic highs, such as salt diapirs and the Senja Ridge (Figure 6). The model expression with ca. 50% error at well 7016/2-1 largely matched stratigraphically with the seismic profile showing a thin lower Eocene

unit around the marginal high (Figure 6; Lasabuda, Laberg, Knutsen, & Høgseth, 2018).

A shale-dominated succession characterizes most of the study area (Figure 5a). Sandstone occurrences are constrained to bathymetric lows adjacent to local slopes (Figures 5b and 6). The sediment distribution is in agreement with generally fine-grained lithologies occurring in the western basins based on well data (Eidvin et al., 2022; Ryseth et al., 2003), which corresponds to deep marine paleobathymetric setting (Lasabuda et al., 2023).

4.2 | Middle Eocene (ca. 47–33 Ma)

In the middle Eocene, major increases in sediment supply (Q_s) were set from S1/Greenland ($500\,km^3$/Ma) and S2/Stappen High ($400\,km^3$/Ma) together with moderate input from S3/Undifferentiated eastern source ($200\,km^3$/Ma) and low input from both S4/Loppa High and S6/Fennoscandia ($10\,km^3$/Ma) (Table 1; Figures S6–S10). The water discharge (Q_w) was set to be high from both S3/Undifferentiated eastern source ($800\,m^3$/s) and S2/Stappen High ($600\,m^3$/s), and moderate flux from S1/Greenland ($200\,m^3$/s) and low input from both S4/Loppa High and S6/Fennoscandia ($10\,m^3$/s) for the duration of 14 million years during the middle–late Eocene (47–33 Ma) (Figure 4d; Figures S6–S10).

Our model shows thicknesses of 406 m, 2059 m and 161 m compared to actual middle Eocene formation thicknesses of 723 m, 1810 m and 109 m at the location of wells 7216/11-1S, 7316/5-1 and 7016/2-1, respectively (Figures 5a,b and 6). In well 7216/11-1S in the Sørvestsnaget Basin, the model shows a thickness discrepancy of 43% (Figure 5a). However, the large-scale stratigraphic trend shows a similarity of thick middle Eocene strata indicating major deposition in the basin (Figure 5a).

In well 7316/5-1 in the Vestbakken Volcanic Province, the simulation managed to produce a low thickness error of only 13.7%, which strongly mimics the seismic profile that shows very thick middle Eocene strata, i.e., >1800 m (Figure 5b). However, the model failed to match the thickness at well 7016/2-1 at Harstad Basin (2.5× thicker than the actual formation). Despite this detailed and local discrepancy, the SFM shows a comparable stratigraphic expression of thin middle Eocene in the marginal high area (Figure 6).

Fine- to medium-grained sands were concentrated in the central part of Sørvestsnaget Basin in the vicinity of well 7216/11-1S (Figures 5a and 7a). The fan-lobe system was modelled with direct sand delivery from a clinoform system that has been sourced from S3 (Figures 4d and 7a). The modelled sandy lobes did not reach far south, which is confirmed by shale-rich succession in well 7016/2-1 in Harstad Basin (Figure 7a; Blaich et al., 2017). Moreover, the modelled middle Eocene succession is relatively thin
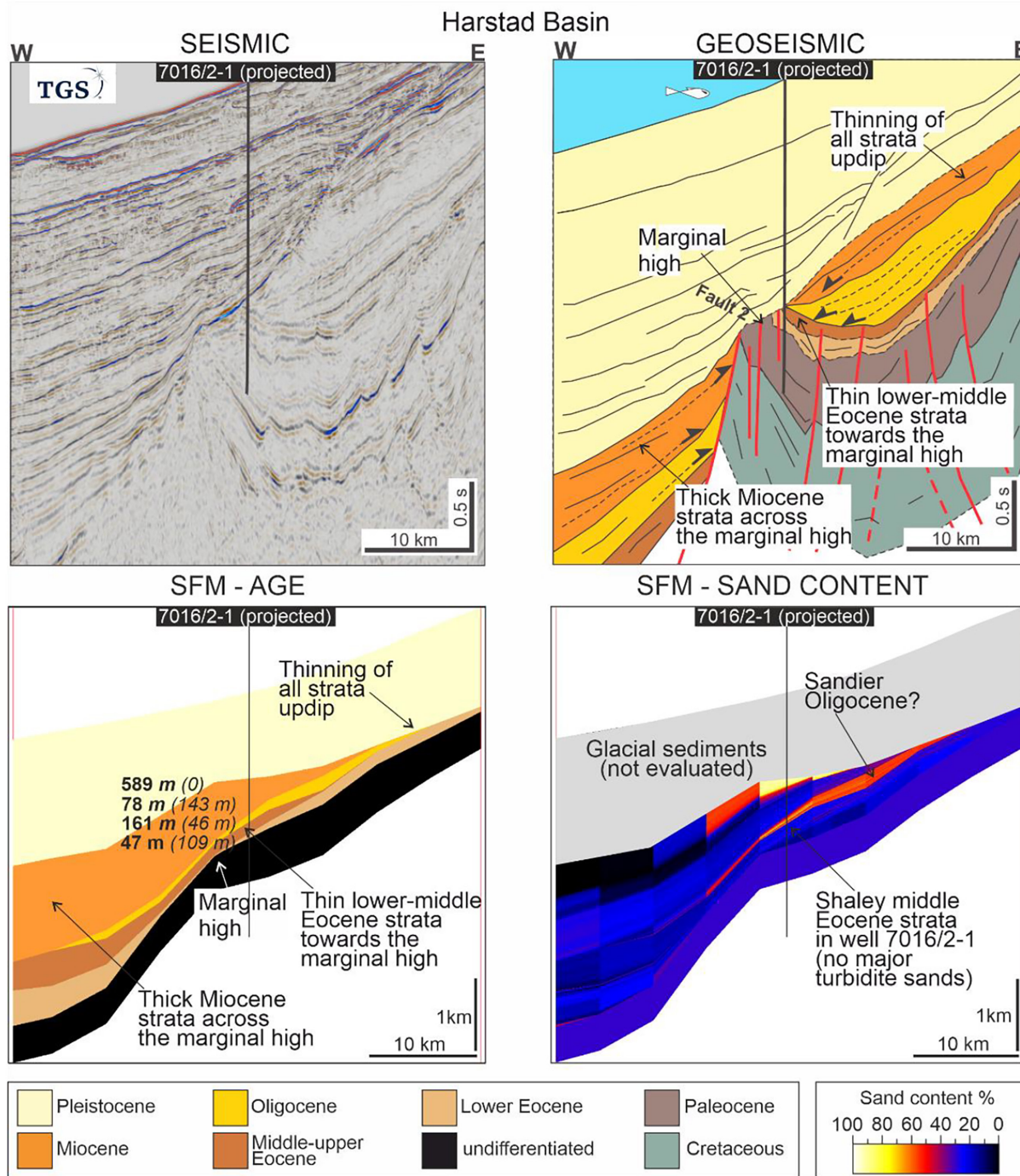
FIGURE 6 The comparison between seismic, geoseismic of Lasabuda, Laberg, Knutsen, and Høgseth (2018), SFM result showing age and SFM result showing sand content for the Harstad Basin (VE: 7×). At the well location, the thickness of each depositional unit (i.e. lower Eocene, middle Eocene, Oligocene and Miocene) from the model is shown in bold, while thickness based on formation well tops is shown in (*italic*). For the location of the seismic profile, see Figure 1b.

with low porosity around the location of this well, which may suggest a very low input from the Fennoscandian source area (Figures 4d, 7b,c).

The modelled middle Eocene system shows a similar thickness trend as that derived from the seismic data (Figure 7c–e). A major increase os sediment thickness in the southwestern part may be related to a depocentre developing towards the oceanic Lofoten Basin (Figure 7c,d).

Upper Eocene sandy units may be present in the Sørvestsnaget Basin, particularly against the salt diapir and the Senja Ridge (Figure 5a). In the Vestbakken Volcanic Province, the middle Eocene succession is thick (>2 km) and dominated by shale with layers of sandstone
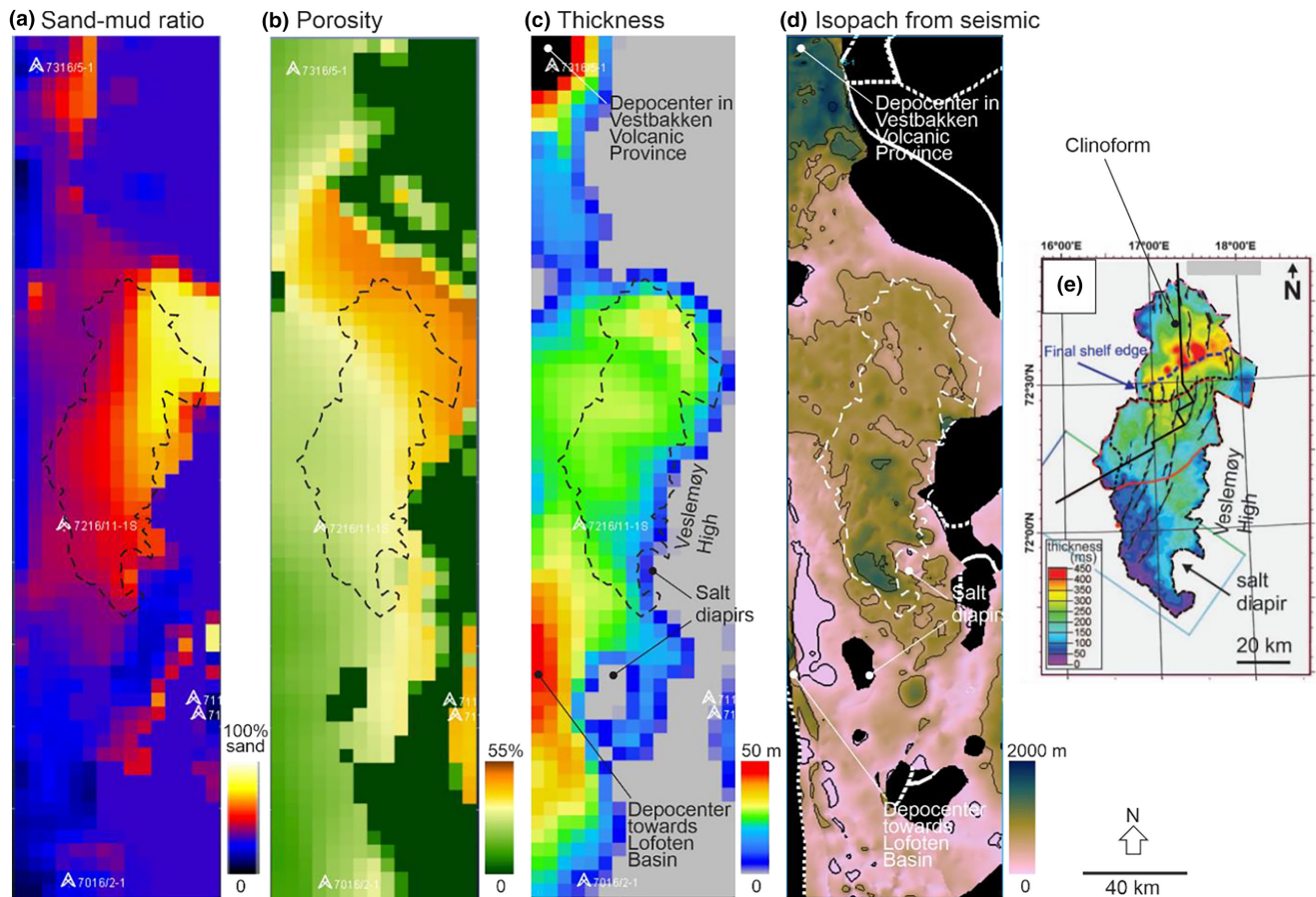
FIGURE 7 The best-fit model for the middle Eocene depositional system showing (a) the sand-mud ratio, (b) porosity variation, (c) thickness distribution, in comparison with (d) thickness map of the middle Eocene from Lasabuda, Laberg, Knutsen, and Høgseth (2018) and (e) thickness map of the upper sequence of the middle Eocene prograding wedge and depositional system of Safronova et al. (2014). The dashed line is the outline of the middle Eocene depositional system from Safronova et al. (2014). Note that the thickness maps shown in (d) and (e) are meant for overall comparison and do not represent the exact same sequence with thickness in the model (c).

of the middle Eocene age (Figure 5b). These sandy packages at well 7316/5-1 may represent turbidites from the nearby Stappen High (Eidvin et al., 2022).

4.3 | Oligocene (ca. 33–23 Ma)

A major reduction in sediment supply (Q_s) and water discharge (Q_w) was set for the Oligocene period spanning 10 million years from 33 to 23 Ma to mimic the thin Oligocene succession in the study area (Table 1). Main sediment directions remain coming from S2/Stappen High (Q_s: 30 km^3/Ma and Q_w: 20 m^3/s) and S3 (Q_s: 10 km^3/Ma and Q_w: 20 m^3/s), S4/Loppa High (Q_s: 40 km^3/Ma and Q_w: 30 m^3/s), and S5/Undifferentiated eastern source (Q_s: 30 km^3/Ma and Q_w: 20 m^3/s) (Figure 4e; Figures S11–S14). Zero sediment input was modelled from S1/Greenland and S6/Fennoscandia (Figure 4e).

At the location of wells 7216/11-1S, 7316/5-1 and 7016/2-1, our model shows thicknesses of 0 m, 153 m and

78 m while the Oligocene strata at these wells show thicknesses of 98 m, 130 m and 143 m, respectively (Figures 5a,b and 6). There has been a major thickness reduction in the Oligocene strata compared to the underlying middle Eocene (from 723 m to 98 m at well 7216/11-1S, or from 1810 m to 130 m at well 7316/5-1). The model is able to capture a similar significant reduction trend from the middle Eocene to Oligocene (from 406 m to 0 m at well 7216/11-1S, or from 2059 m to 130 m at well 7316/5-1) (Figure 5a,b).

Moreover, we observe comparable sedimentation patterns imaged on seismic data, for example very thin Oligocene strata at the Sørvestsnaget Basin but relatively thicker strata on the flanks of salt diapirs (Figure 5a,b). The majority of deposition occurred in the Vestbakken Volcanic Province and the northern part of the Sørvestsnaget Basin near the "Knølegga" structure (Figure 5b). At well 7016/2-1 in the Harstad Basin, the model gives a ca. 45% thickness difference against the actual Oligocene formation. However, the SFM managed to capture the overall thinning of the strata updip of the basin (Figure 6). Much

of the modelled Oligocene succession appears to be mud-dominated as the sandier parts have been deposited to the east for example, in the Harstad Basin (Figure 6).

4.4 | Miocene (ca. 23–2.7 Ma)

Sediment supply (Q_s: 10–25 km^3/Ma) with water discharge (Q_w: 5–20 m^3/s) from the east was set to fill the basin (Figure 4f; Figures S15–S19). This sediment input configuration reflects the complex pattern of sedimentation during the Miocene. Northern sediment supply (i.e. S1/Greenland) and southern sediment supply (i.e. S6/Fennoscandia) were set to be inactive (Table 1).

Our model shows thicknesses of 7 m, 432 m and 589 m compared to actual Miocene formation thicknesses of 100 m, 11 m and 0 m at the location of wells 7216/11-1S, 7316/5-1 and 7016/2-1, respectively (Figures 5a,b and 6). Differential deposition appears on the flank of the salt diapir and the marginal high, accompanied by a major accumulation in the Vestbakken Volcanic Province and the Harstad Basin (Figures 5a,b and 6). The Miocene model shows 14x thinner and 40x thicker than the actual formation thickness found at the well 7216/11-1S in Sørvestsnaget Basin and at the well 7316/5-1 in Vestbakken Volcanic Province, respectively (Figure 5a,b). This large discrepancy the Vestbakken Volcanic Province may be due to loss of sediment towards the wider part of the province and the Lofoten Basin. However, the overall pattern of the Miocene is still analogous to the seismic profile, for example, a relatively thin Miocene strata in the Sørvestsnagen basin and a truncation of the strata towards the Knølegga structure (Figure 5a,b).

In the Harstad Basin, specifically at the well 7016/2-1 location, the model produced very thick strata (>500 m) and failed to onlap towards the marginal high (Figure 6). However, this thick Miocene succession is identical as observed on the seismic data representing deposition towards the Lofoten Basin (Figure 6). A predominant shale succession shows similarities to the mudstone-dominated contourite deposits reported in wells 7216/11-1S and 7316/5-1 (Figure 5a,b; Rydningen et al., 2020). A sandier Miocene model is observed in the central part of the Sørvestsnaget Basin (Figure 5a).

5 | DISCUSSION

5.1 | Sensitivity test of K_w sand values against sand content (%)

Following our modelling results presented above, we run sensitivity tests using middle Eocene source-to-sink parameters because this system is well-constrained and

host several key sedimentary features including mapped clinoform successions and drilled submarine fans (Ryseth et al., 2003; Safronova et al., 2014).

Regarding diffusion coefficient (K), we tested ranges of values for marine conditions (K_w) for sand. The tested K_w values for sand were 0.1, 1 and 3 as these numbers are considered suitable in typical large-scale passive margins (Hawie et al., 2017). The K_w value of 5 for marine shale was suggested as an optimum value (Barabasch et al., 2019; Hawie et al., 2017) and K_w for continental sand and shale of 50 and 500 were computed following Gervais et al. (2023).

We plotted K_w sand values against sand content of 25%, 50% and 75% (Figure 8). K_w sand value of 0.1 regardless of the sand content shows sand redistribution to the north, instead of to the well 7216/11-1S (Figure 8a,d,g). K_w sand value of 1 produced inconsistent models of dominant sediment accumulation trend towards the west and slightly to the north (Figure 8b,e,h). However, the model with K_w sand value of 1 and sand content of 50% and 75% generated sandy accumulation that reached the vicinity of well 7216/11-1S (Figure 8e,h). Models using K_w value of 3 were able to redistribute the sand generally to the south (Figure 8c,f,i), particularly with higher sand content, that is, 50%–75% (Figure 8f,i). A high sand content is common when the model specifically targets submarine fans (e.g. Hawie et al., 2018).

The sensitivity analysis above shows the role of the diffusion coefficient for marine conditions (K_w) in the diffusion equation used in DionisosFlow SFM. The K_w coefficient represents a key control on the transferability of sand reflecting on the spatial distribution of the sandy deposits (Figure 8). The bigger the K_w value, the further the sandy deposits can be transported effectively underwater, which agrees with other SFM studies (e.g. Barabasch et al., 2019; Hawie et al., 2017).

5.2 | Sensitivity test of sediment load—Q_s (km^3/Ma) against water discharge—Q_w (m^3/s)

We tested relationships between sediment load (Q_s) and water discharge (Q_w) (Figure 9). Low, medium and high Q_s values are represented by 20, 200 and 1000 km^3/Ma, while low, medium and high Q_w values are represented by 80, 800 and 2800 m^3/s (Figure 9). As a reference, the Nile River sediment load (Q_s) is around 1400 km^3/Ma with water discharge (Q_w) of around 2800 m^3/s, while the Saudi Arabian and Latakia sediment loads (Q_s) are around 650 and 300 km^3/Ma with water discharges (Q_w) around 800 and 80 m^3/s, respectively (e.g. Figure S1; Hawie et al., 2017).

Low Q_s models failed to transfer sand to the central part of the Sørvestsnaget Basin (Figure 9a,d,g). Although high Q_w might have facilitated the sand transfer, given the
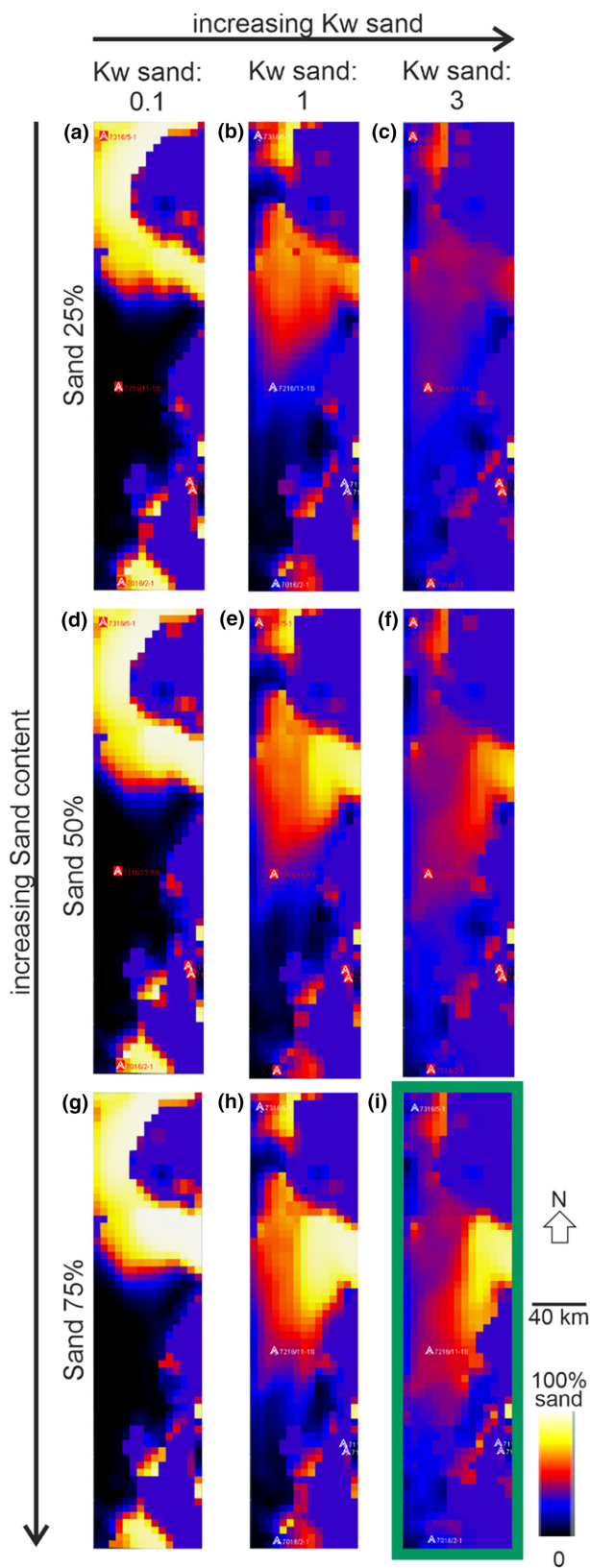
increasing Kw sand →

FIGURE 8 Sensitivity test of K_w sand values against sand content (%). (a) K_w sand 0.1 and sand 25%; (b) K_w sand: 1 and sand 25%; (c) K_w sand: 3 and sand 25%; (d) K_w sand 0.1 and sand 50%; (e) K_w sand: 1 and sand 50%; (f) K_w sand: 3 and sand 50%; (g) K_w sand: 0.1 and sand 75%; (h) K_w sand: 1 and sand 75%; and (i) K_w sand: 3 and sand 75% show the best-fit model (green rectangle).

Medium Q_s (200 km³/Ma) simulations resulted in the best-fit reconstructions (Figure 9b,e,h). This value is equivalent to other systems, such as the Late Triassic of the Barents Shelf (Gilmullina et al., 2022) and the modern continental margin of the Canadian Arctic (Milliman & Farnsworth, 2013). The model with medium Q_s and medium Q_w (800 m³/s) shows the likely scenario for the middle Eocene system (Figure 9e). High Q_s (1000 km³/Ma) models show too much sand in the basin and an unrealistic sand distribution pattern, which is also in contrast with well 7216/11-1S (Figure 9c,f,i). A comparable relation between Q_s and Q_w has been reported from modern systems in upland areas with relief of 200–600 m with a typical drainage area of 7000–9000 km² (Figure S8; Milliman & Syvitski, 1992) as well as ancient systems, such as the Cretaceous Humber Valley, Canada (Sangster et al., 2019).

Using parameters similar to the ones presented in Figure 9, the model with low Q_s and low Q_w shows too thin strata (Figure 10a). If we increase the sediment load (Q_s) just to a medium level, the thickness expands to an acceptable thickness using medium Q_w (Figure 10b). If we raise the sediment load (Q_s) value to a higher level, even with low Q_w, the resulting thickness of the model is even higher (Figure 10c). This means that the water discharge (Q_w) did not play a major role in thickening the basin fill strata. However, this parameter is subjected to rainfall and evapotranspiration rates, which can be varied in different climate systems (Eide et al., 2018).

5.3 | Sensitivity test of sediment load— Q_s (km³/Ma) against precipitation and evaporation (mm/year): The role of climate on sediment transfer

We ran another test between Q_s and climate, represented here by precipitation and evaporation (mm/year). Precipitation and evaporation values were set to three different values: low (130 and 140 mm/year), medium (1300 and 1400 mm/year) and high (3900 and 4200 mm/year) (Figure 11). Model of low Q_s and low precipitation and evaporation shows not enough sand to be distributed (Figure 11a). By increasing the precipitation and evaporation, low Q_s models were able to change the transport direction of sediments southwards, although they were still not sufficient to transport sediments to the south

climate of the system in the middle Eocene, it is unlikely that such high sediment discharge equivalent to for example the Nile River (i.e. major low-latitude rivers) occurred in the study area (Figure 9g; Milliman & Meade, 1983).
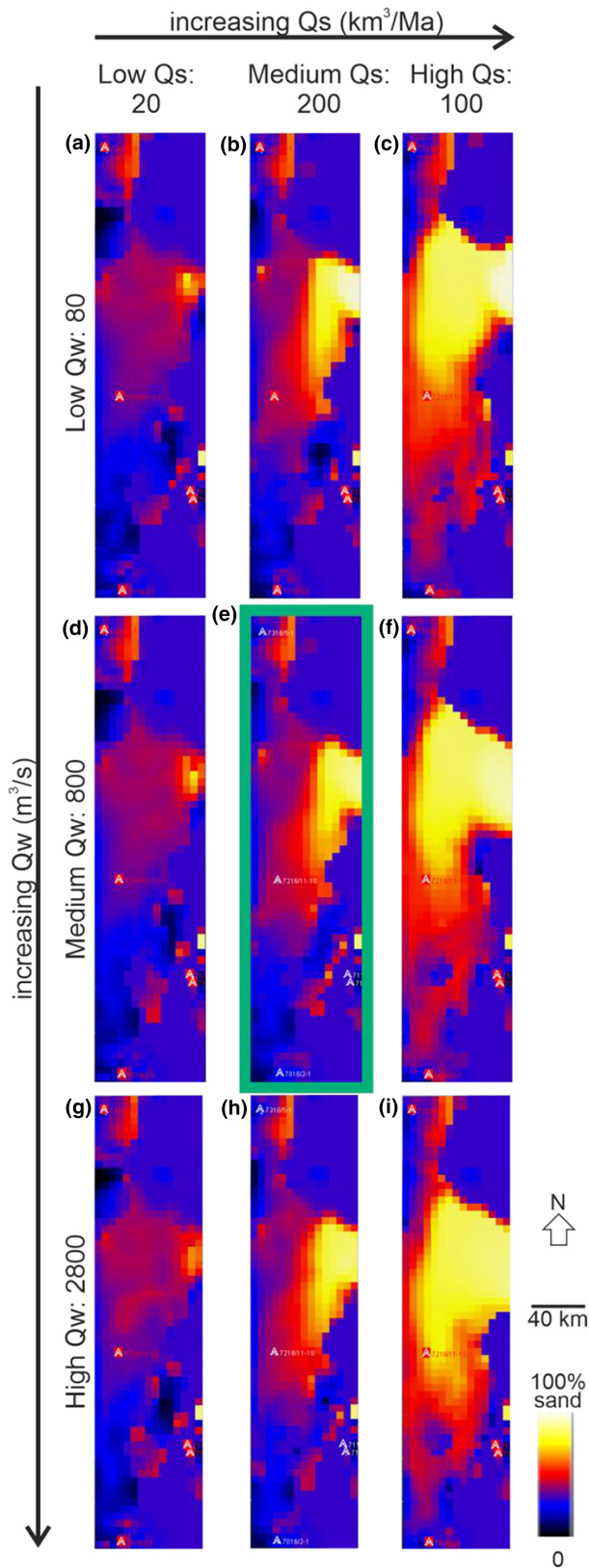
FIGURE 9 Sensitivity test of Q_s (km^3/Ma) against Q_w (m^3/s). (a) Q_s: 20 and Q_w: 80; (b) Q_s: 200 and Q_w: 80; (c) Q_s: 1000 and Q_w: 80; (d) Q_s: 20 and Q_w: 800; (e) Q_s: 200 and Q_w: 800 show the best-fit model (green rectangle); (f) Q_s: 1000 and Q_w: 800; (g) Q_s: 20 and Q_w: 2800; (h) Q_s: 200 and Q_w: 2800; and (i) Q_s: 1000 and Q_w: 2800.
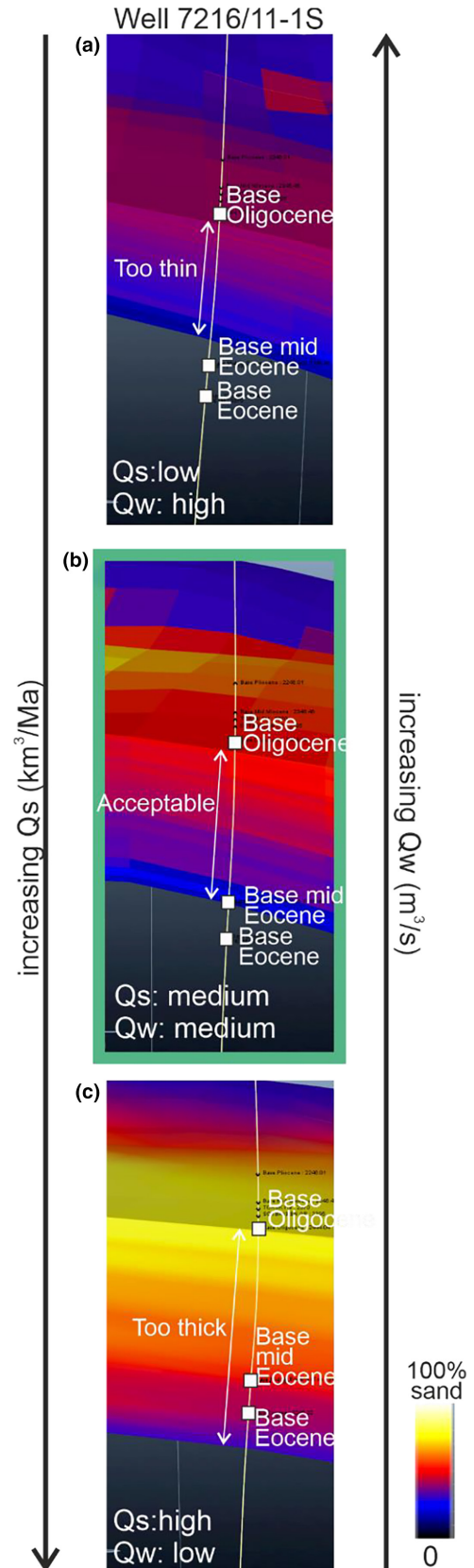

FIGURE 10 Thickness comparison of models against formation well tops from well 7216/11-1S. (a) Low Q_s and high Q_w; (b) Medium Q_s and medium Q_w are the best-fit parameters (green rectangle); and (c) High Q_s and low Q_w.
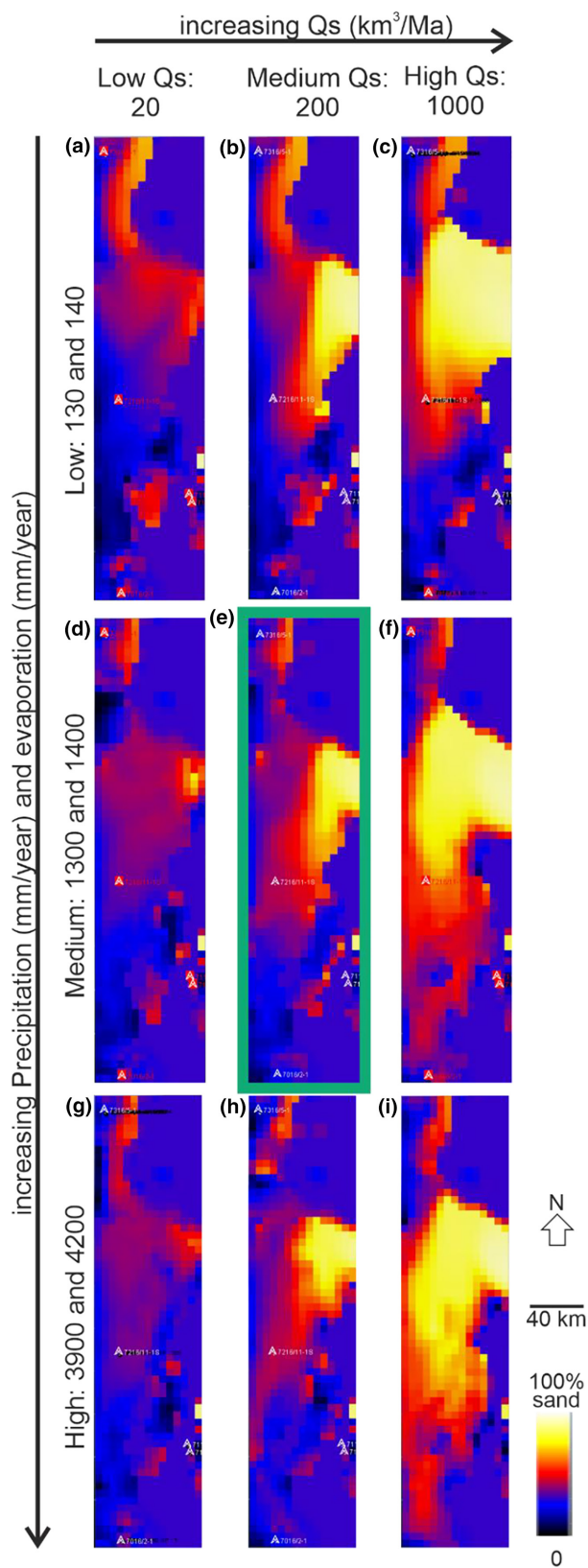
FIGURE 11 Sensitivity test of Q_s (km^3/Ma) against precipitation (Pr) and evaporation (Ev) (mm/year). (a) Q_s: 20, Pr: 130, Ev: 140; (b) Q_s: 200, Pr: 130, Ev: 140; (c) Q_s: 1000, Pr: 130, Ev: 140; (d) Q_s: 20, Pr: 1300, Ev: 1400; (e) Q_s: 200, Pr: 1300 and Ev: 1400; (f) Q_s: 1000, Pr: 1300, Ev: 1400; (g) Q_s: 20, Pr: 3900, Ev: 4200; (h) Q_s: 200, Pr: 3900, Ev: 4200; and (i) Q_s: 1000, Pr: 3900, Ev: 4200.

The low value of precipitation and evaporation (Figure 11a–c) is in the same order as in Antarctica, ca. 200 mm/year (Palerme et al., 2017), which is unlikely to occur in the study area where moderately temperate climate occurred in the early to middle Eocene (Golovneva et al., 2023; Helland-Hansen & Grundvåg, 2021; Uhl et al., 2007) with a precipitation rate analogues to the Eocene of Arctic Canada, ca. 930–1900 mm/year (Greenwood et al., 2010; Schubert et al., 2012). In addition, high values of precipitation are similar to tropical rainforest climate, which is also unlikely for the middle Eocene system (Figure 11g,h,i). Therefore, a model with medium Q_s and medium precipitation and evaporation is considered the best-fit simulation (Figure 11e).

Based on our modelling, there is no clear trend of more effective sediment transport to the basin when we increase the level of precipitation and evaporation (e.g. Figure 11a,d,g). However, the climatic component addressed here does not seem to have a dominant role in increasing sand transport compared to the sediment load (Q_s) (c.f. Figure 11d–f). High precipitation values are commonly associated with wet climate that results in high riverine runoff, that is, a ratio of annual river discharge to drainage area (Eide et al., 2018; Milliman & Farnsworth, 2013). In the case of climate change where temperature rises, evaporation is expected to increase and in turn, produce higher precipitation (Dai et al., 2018; Trenberth, 2011) resulting in much more dynamic sediment distribution (Figure 11g,h,l) as also observed in studies specifically addressing PETM systems (e.g. Colombera et al., 2017; Sømme et al., 2023).

5.4 | Sensitivity of directions and magnitudes of source areas

We tested multiple simulations of basin filling using different source areas (Figure 12). We explore the role of various dominant sources (e.g. Loppa High, Greenland, Fennoscandia) in a multi-source-to-sink scenario. For example, how the model would respond if we increased sediment supply from the Loppa High during the early Eocene and the middle Eocene (Figures S20 and S21). We found that the models show unrealistically high sand content when incorporating the Loppa High as the dominant source (Figures S20 and S21). However,

of the study area (Figure 11a,d,g). Medium Q_s models seem better at delivering sediment to the starved basin (Figure 11b,e,h) while simulations with high Q_s values produced unrealistically too sandy models for the study area (Figure 11c,f,i).
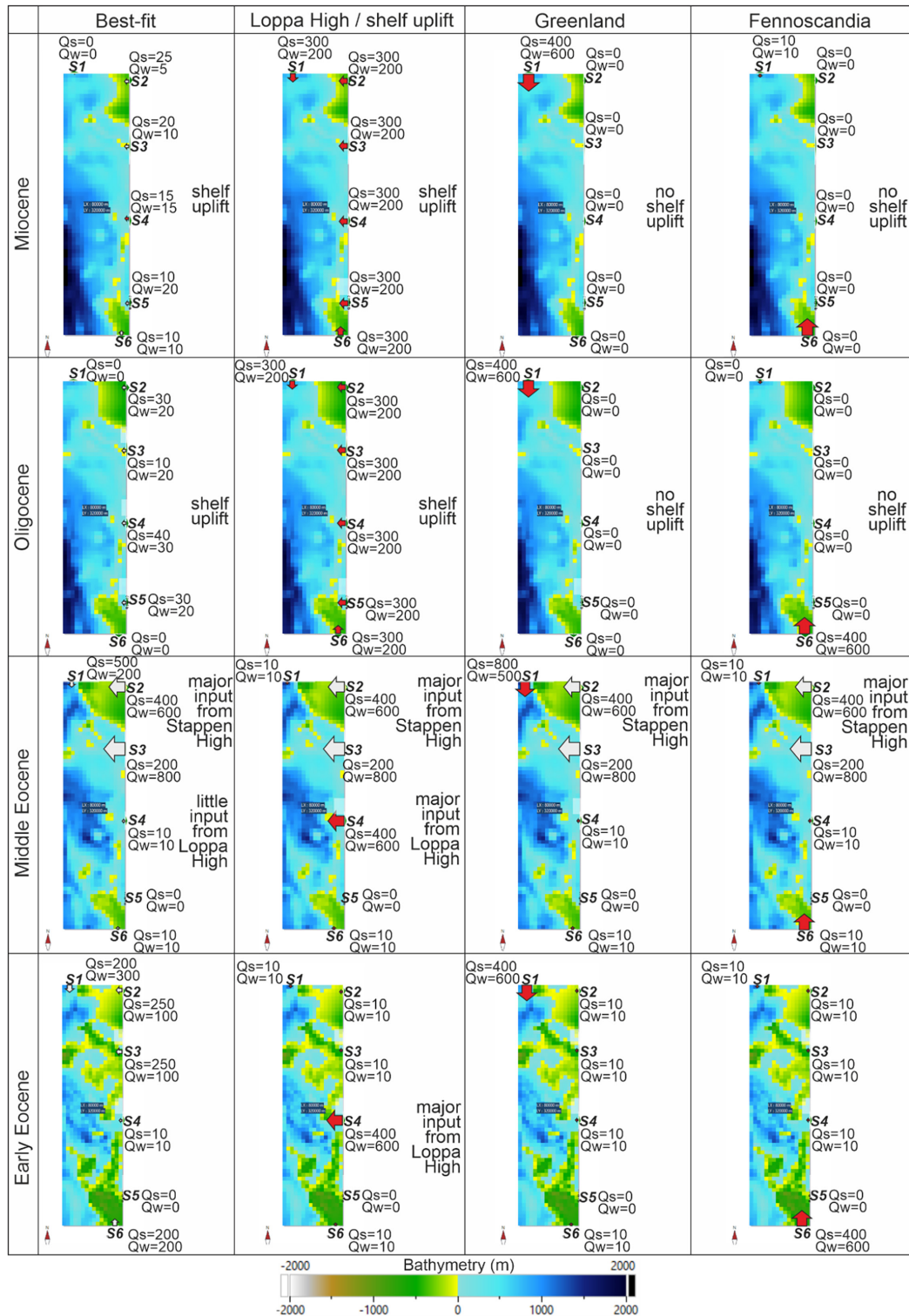
FIGURE 12 Summary of sensitivity test using different directions and magnitude of source areas. Best-fit sediment supply as shown in Figure 4 is compared against a single dominant source area. For more information on the resulting models, see Figures S20–S23.

input from the Loppa High area would be important during the Oligocene and Miocene (Figures S22 and S23). Sediment contribution from the Loppa High was also recorded during the Early Cretaceous, evidenced by the deposition of submarine fans in the Hammerfest

Basin (Harishidayat et al., 2018; Marín et al., 2018), possibly as a response to an uplift episode of the Loppa High (Indrevær et al., 2018).

Greenland was a key source area for parts of the Barents Shelf during the Early Cretaceous (e.g. Grundvåg

et al., 2017), a period long before the time intervals modelled here. Our simulation shows that this source area was still relevant during the early Eocene (Figure S20) considering a relatively close distance from Greenland's shoreline to the study area (<50 km) (Figure 2a; Lasabuda, Laberg, Knutsen, & Safronova, 2018). Increased sediment supply from Greenland shows moderate impact, particularly on the middle Eocene model in which the flow would have restricted submarine fan distribution (Figure S21). However, the scenario of higher input from Greenland has little consequences for the Oligocene and Miocene models (Figures S22 and S23). This scenario may be unlikely considering the geographical position of Greenland's coastline in the Oligocene and Miocene relative to the study area (>200 km), which is an uncommon dimension of a shelf width for a typical large passive margin classified by Nyberg et al. (2018) (see Figure 2c,d; Lasabuda, Laberg, Knutsen, & Safronova, 2018).

Increasing supply of sediments from Fennoscandia apparently contributed to major deposition of mud in the study area (Figures S21–S23). This shows the importance of Fennoscandia as a sediment source of fine-grained clastics as also documented in the Mesozoic basin fill sequences of the southern Barents Shelf (Gilmullina et al., 2022; Grundvåg et al., 2017; Klausen et al., 2017). However, it seems unlikely that Fennoscandia acted as the main drainage basin in the Cenozoic multi-source-to-sink system of the SW Barents Shelf (see below). This view is supported by lithological differences between Fennoscandia where igneous and metamorphic rocks are dominating, thus contrasting the more erodible sedimentary rocks of the Barents Shelf (Henriksen, Ryseth, et al., 2011; Ramberg, 2008).

A sub-crop map at the different times modelled would have helped to understand what kind of sediment was subject to erosion. However, there are no such detailed maps available for the Eocene, Oligocene, and Miocene periods except the present-day sub-crop map below Quaternary sediment compiled by Henriksen, Bjørnseth, et al. (2011). The key reason is that the Paleogene–Neogene sedimentary successions are very limited in the Barents Sea area and were largely eroded during the Quaternary (e.g. Lasabuda et al., 2021; Smelror et al., 2009).

5.5 | Implications for Cenozoic sediment routing

5.5.1 | Early Eocene (ca. 55–47 Ma)

In the early Eocene, sediments from the northeast were likely coming from an uplifted area along the

northwesternmost margin of the Barents Shelf (Figure 13a) as a result of the Eurekan deformation, which also was responsible for the development of the West Spitsbergen fold-and-thrust belt (Dimakis et al., 1998; Henriksen, Bjørnseth, et al., 2011; Piepjohn et al., 2016). An early Eocene paleotopographic model and paleostress simulation also suggest regional uplift of the northern Barents Shelf (Gac et al., 2020; Rasmussen & Fjeldskaar, 1996). Some considerable portions of the sediments might have come from the nearby Stappen High and the southern source (i.e. Fennoscandia), thus being in agreement with the regional source-to-sink model of Lasabuda, Laberg, Knutsen, and Høgseth (2018). However, the present model shows that the Loppa High was, most likely, not a principal sediment source (Figure 12). This result may be explained by a structural reconstruction of Indrevær et al. (2018) based on metamorphic phase changes showing that the Loppa High was part of a broader, submerged shelf in the Paleocene and the early Eocene. Our model also supports sediment routing from Greenland through the Norwegian-Greenland Sea, which was very narrow, during the Eocene based on provenance analysis using zircons and minerals from well data by Flowerdew et al. (2023) (Figure 13a).

The early Eocene highstand shows the highest sea level (up to 120 m) throughout the modelled periods (Figure 3b). This may have consequences on the pattern of sediment supply through the simulated source outlets (Covault et al., 2011; Nyberg et al., 2018; Sømme, Helland-Hansen, Martinsen, & Thurmond, 2009). The central part of the Barents Shelf was likely a wide shelf (>50 km) in a typical large passive margin (sensu Sømme, Helland-Hansen, Martinsen, & Thurmond, 2009), which may have severely been impacted by relative sea-level fluctuations compared to a narrower shelf in tectonically active systems (Nyberg et al., 2018). The paleo shelf to the east (including the Loppa High area) may have formed a temporary sink/storage before it eventually remobilised the sediments to the basin floor during subsequent sea level fall (e.g. Romans et al., 2016). This configuration resulted in lower sediment contribution from the east and a more dominant supply from the Stappen High and northeastern sources (Figure 13a).

5.5.2 | Middle Eocene (ca. 47–33 Ma)

Our best-fit simulation for the middle Eocene shows that there was significant input from the Stappen High and northeastern Barents Shelf areas (Figure 13b). This result fits well with an uplift configuration which shows major topographic highs in the north and northeast of the Barents Shelf (Lasabuda, Laberg, Knutsen,
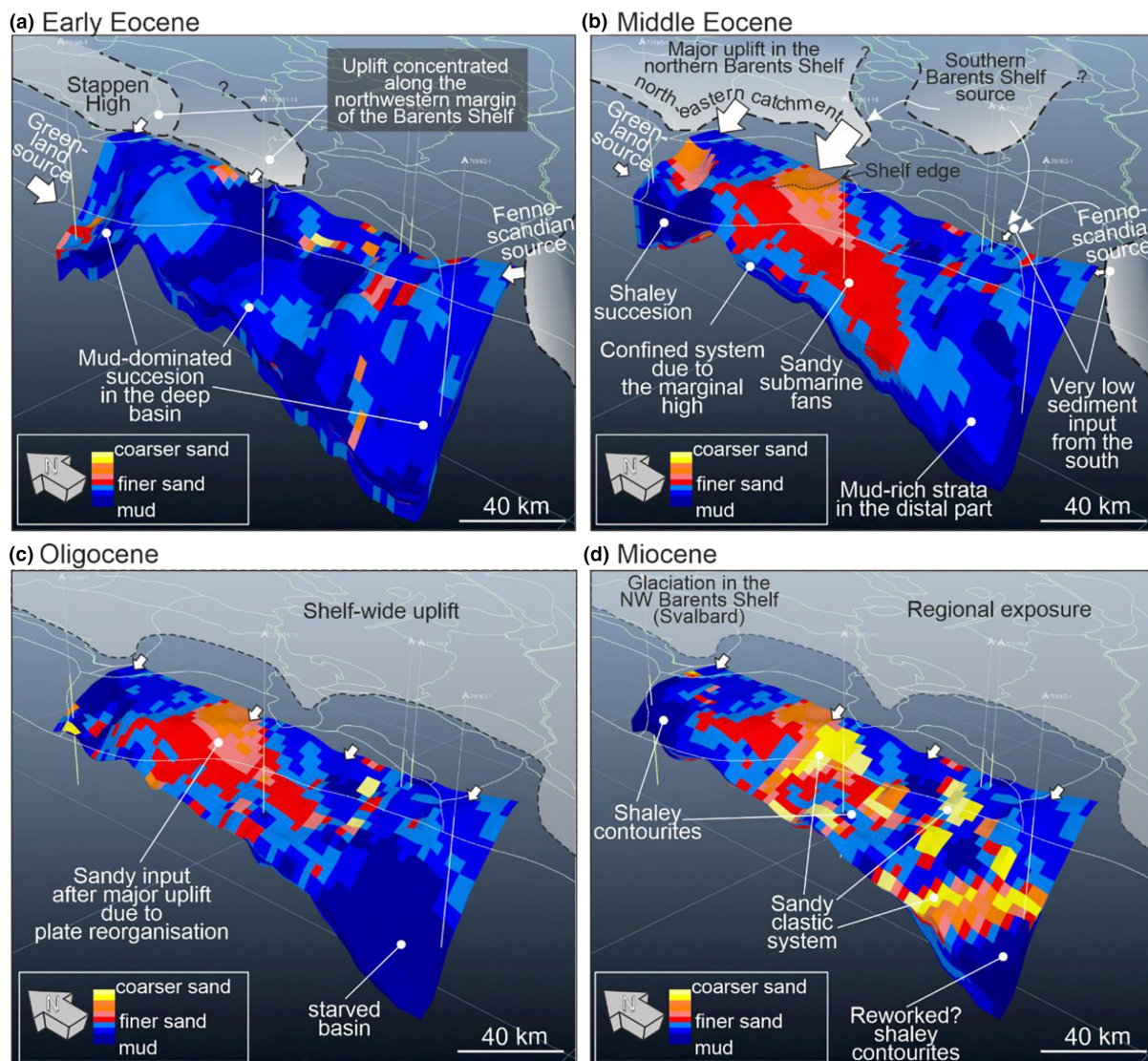
FIGURE 13 Paleo-source areas (dashed grey areas) and depositional sink in the SW Barents Sea for (a) Early Eocene; (b) Middle Eocene; (c) Oligocene and (d) Miocene. Delineation of source areas (Lasabuda, Laberg, Knutsen, & Høgseth, 2018; Smelror et al., 2009) and middle Eocene sediment routing based on the recent provenance study of Flowerdew et al. (2023) are shown. Note that these figures are 3-D views.

& Høgseth, 2018; Smelror et al., 2009). The sedimentation pattern in the Vestbakken Volcanic Province was dominated by mud with some sandy turbidites from the Stappen High area (Figure 13b). These muds were likely derived from Greenland representing a long-distance transport based on a provenance study by Flowerdew et al. (2023).

A major sea-level fall in the middle Eocene has been attributed to the tectonic uplift, which may have resulted in the drainage reorganisation of the source areas involved (e.g. Covault et al., 2011). Our study also suggests a slight increase in sediment supply from the southeastern Barents Shelf. This means that the catchment areas might have been larger in the eastern and northeastern Barents Shelf in the middle Eocene compared to the early Eocene

(Figure 13a,b). The potential expansion of drainage areas including the Greenland source (Figures S6–S10) resulted in major sediment deposition in the Central Tertiary Basin on Spitsbergen (Helland-Hansen & Grundvåg, 2021; Petersen et al., 2016; Plink-Björklund, 2020). This major sea-level fall would also impact the distance from the paleoshoreline to the shelf edge, which may promote the deposition of gravity-driven deposits (e.g. Pellegrini et al., 2018). Our model also agrees that the clinoforms and sandy submarine fans found in well 7216/11-1S were likely coming from a north to northeastern source (Safronova et al., 2014).

The drainage reorganisation may include the emergence of the southern Barents Shelf source that may have contributed to the increase of sediment supply sourced

from the east (Figure 13b). However, the sediment supply from the Loppa High which may have been reworked and mixed with sediments from Fennoscandia as suggested by Flowerdew et al. (2023) is estimated to be relatively limited according to our simulation (Figure 13b). Regional seismic mapping by Blaich et al. (2017) and Lasabuda, Laberg, Knutsen, and Høgseth (2018) show no obvious sediment progradation from the Loppa High compared to the Stappen High, which may explain the small contribution of sediments in the model.

5.5.3 │ Oligocene (ca. 33–23 Ma)

In the Oligocene, major amounts of sediment were sourced from the east with contributions from the Stappen High, Loppa High and Fennoscandia (Figure 13c). These source areas represent a shelf-wide uplift and might have been a continuous source area during the Oligocene (Lasabuda, Laberg, Knutsen, & Safronova, 2018). This uplift has been attributed to a deeper mantle process due to plate reorganisation (Lasabuda et al., 2021) and is suggested to be a regional event across the Arctic (Green & Duddy, 2010). The regional exposure may be amplified by major sea-level fall at the onset of the Oligocene which has been attributed to the global climate deterioration evidenced by the growth of the Antarctic ice sheet (Westerhold et al., 2020; Zachos & Kump, 2005). Deposition from Greenland was likely very limited or absent due to a distant paleogeographical location of Greenland relative to the Barents Shelf (see above) due to seafloor spreading and passive margin development (Doré et al., 2016; Faleide et al., 2008). Fennoscandia may have provided sediments to the SW Barents Shelf, but this was likely not significant based on our model.

5.5.4 │ Miocene (ca. 23–2.7 Ma)

In the Miocene, limited sediment supply (Q_s: 10–25 km^3/Ma) might be related to the low sediment input from the eastern source area (Figure 13d). This is likely because the Barents Shelf was not opened for ocean connection until sometime in the Quaternary (Lasabuda et al., 2023). However, the sediment input could have been larger but then redistributed by the ocean currents flowing to the north, or it was transferred to the deep Lofoten Basin (not captured in the extent of the study area). Our simulation shows no or very little sediment input from the north, which is in agreement with the paleocurrent direction going from south to north in the Miocene (Jakobsson et al., 2007). Although the model did not consider sediment input from the south, we do not exclude a fraction

of fine-grained sediment from the south that might be transported through ocean currents (e.g. Bjordal-Olsen et al., 2022; Laberg et al., 1999).

Sea-level fluctuations throughout the Miocene are estimated to be in the order of 30 m (Miller et al., 2005, 2020). This may have implications for the deposition of contourites on the slope, that is, the Bjørnørenna Drift may have been extended landward during sea-level rise in this period (Rydningen et al., 2020). Major sea-level falls at the end of the Miocene coupled with early Pliocene uplift (Knies et al., 2014) may explain a generation of ice sheet build-up for the Quaternary glaciations (e.g. Laberg et al., 2012; Patton et al., 2022).

6 │ CONCLUSIONS

We have applied SFM to simulate basin filling in the SW Barents Shelf for the early Eocene (ca. 55–47 Ma), middle Eocene (ca. 47–33 Ma), Oligocene (ca. 33–23 Ma) and Miocene (ca. 23–2.7 Ma). Our study shows the following,

1. The pattern of sedimentation in the SW Barents Sea did not specifically point to a single source, but from a multi-source sediment transfer. Best-fit models for the SW Barents Sea multi-source-to-sink using diffusion coefficient (K_w) sand of 3, medium sediment load (Q_s) and medium water discharge (Q_w). However, water discharge (Q_w) appears less sensitive compared to sediment load (Q_s) in transferring sand to the deeper basin.
2. Increasing the level of precipitation and evaporation does not always correspond to the efficiency of sand transport, which indicates a more dynamic sediment distribution pattern depending on the magnitude of sediment supply.
3. The early Eocene model shows relatively equal sediment input from the north, east and south. This suggests an uplifted area that was concentrated along the northwesternmost margin of the Barents Shelf (i.e. Stappen High to Svalbard) and in the Fennoscandian area. This model also supports the transport of sediments from Greenland.
4. In the middle Eocene, our best-fit simulation implies a major sediment supply from the north, northeast and east. Minor input from the north and south is still realistic. In this scenario, the model produced submarine fans similar as imaged in the seismic and well data. Our model agrees with the uplift and erosion pattern of the Stappen High, Greenland/Svalbard and the northern Barents Sea during this period, which shows a dominant sediment input. Our simulation suggests that the southern Barents and Fennoscandia

sources supplied a low sediment flux to the western sink.

5. For the Oligocene and Miocene, a dominant sediment supply from the east is needed to be consistent with seismic and data. Our scenario fits well with the hypothesis of regional shelf-wide uplift of the Barents Shelf, which produces relatively equal sediment input along the eastern sediment outlets.

6. Our SFM results were able to contribute to a better understanding of the dynamic nature and controls of sediment transfer in a multi-source-to-sink system.

CONFLICT OF INTEREST STATEMENT

The authors declare that they have no known competing financial interests or personal relationships that could have appeared to influence the work reported in this paper.

PEER REVIEW

The peer review history for this article is available at https://www.webofscience.com/api/gateway/wos/peer-review/10.1111/bre.12883.

DATA AVAILABILITY STATEMENT

The seismic and well data that support the findings of this study are available through Diskos database of the Norwegian Offshore Directorate (https://www.diskos.com/) and from TGS. The modelling results may be shared from the corresponding author upon reasonable request.

ORCID

Amando P. E. Lasabuda https://orcid.org/0000-0002-8980-3488
Domenico Chiarella https://orcid.org/0000-0003-2482-0081
Sten-Andreas Grundvåg https://orcid.org/0000-0002-4309-898X
Tom Arne Rydningen https://orcid.org/0000-0002-5837-4668
Jan Sverre Laberg https://orcid.org/0000-0003-3917-4895
Alfred Hanssen https://orcid.org/0000-0001-8553-2935

REFERENCES

Amorosi, A., Sammartino, I., Dinelli, E., Campo, B., Guercia, T., Trincardi, F., & Pellegrini, C. (2022). Provenance and sediment dispersal in the Po-Adriatic source-to-sink system unraveled by bulk-sediment geochemistry and its linkage to catchment geology. *Earth-Science Reviews*, *234*, 104202.

Baig, I., Faleide, J. I., Jahren, J., & Mondol, N. H. (2016). Cenozoic exhumation on the southwestern Barents Shelf: Estimates and uncertainties constrained from compaction and thermal maturity analyses. *Marine and Petroleum Geology*, *73*, 105–130.

Barabasch, J., Ducros, M., Hawie, N., Daher, S. B., Nader, F. H., & Littke, R. (2019). Integrated 3D forward stratigraphic and petroleum system modeling of the Levant Basin, Eastern Mediterranean. *Basin Research*, *31*(2), 228–252.

Bergh, S. G., Braathen, A., & Andresen, A. (1997). Interaction of basement-involved and thin-skinned tectonism in the Tertiary fold-thrust belt of central Spitsbergen, Svalbard. *AAPG Bulletin*, *81*(4), 637–661.

Bjordal-Olsen, S., Rydningen, T. A., Laberg, J. S., Lasabuda, A. P., & Knutsen, S.-M. (2022). Contrasting Neogene–Quaternary continental margin evolution offshore mid-north Norway: Implications for source-to-sink systems. *Marine Geology*, *106974*, 106974.

Blaich, O., Tsikalas, F., & Faleide, J. (2017). New insights into the tectono-stratigraphic evolution of the southern Stappen High and its transition to Bjørnøya Basin, SW Barents Sea. *Marine and Petroleum Geology*, *85*, 89–105.

Burgess, P. M., Lammers, H., van Oosterhout, C., & Granjeon, D. (2006). Multivariate sequence stratigraphy: Tackling complexity and uncertainty with stratigraphic forward modeling, multiple scenarios, and conditional frequency maps. *AAPG Bulletin*, *90*(12), 1883–1901.

Colombera, L., Arévalo, O. J., & Mountney, N. P. (2017). Fluvial-system response to climate change: The Paleocene-Eocene Tremp group, Pyrenees, Spain. *Global and Planetary Change*, *157*, 1–17.

Covault, J. A., Romans, B. W., Graham, S. A., Fildani, A., & Hilley, G. E. (2011). Terrestrial source to deep-sea sink sediment budgets at high and low sea levels: Insights from tectonically active Southern California. *Geology*, *39*(7), 619–622.

Dai, A., & Trenberth, K. E. (2002). Estimates of freshwater discharge from continents: Latitudinal and seasonal variations. *Journal of Hydrometeorology*, *3*(6), 660–687.

Dai, A., Zhao, T., & Chen, J. (2018). Climate change and drought: A precipitation and evaporation perspective. *Current Climate Change Reports*, *4*, 301–312.

De Weger, W., Hernández-Molina, F. J., Miguez-Salas, O., De Castro, S., Bruno, M., Chiarella, D., Sierro, F. J., Blackbourn, G., & Manar, M. A. (2021). Contourite depositional system after the exit of a strait: Case study from the late Miocene south Rifian Corridor, Morocco. *Sedimentology*, *68*(7), 2996–3032.

Dimakis, P., Braathen, B. I., Faleide, J. I., Elverhøi, A., & Gudlaugsson, S. T. (1998). Cenozoic erosion and the preglacial uplift of the Svalbard–Barents Sea region. *Tectonophysics*, *300*(1), 311–327.

Doré, A., Lundin, E., Gibbons, A., Sømme, T., & Tørudbakken, B. (2016). Transform margins of the Arctic: A synthesis and re-evaluation. *Geological Society, London, Special Publications*, *431*(1), 63–94.

Dumais, M. A., Gernigon, L., Olesen, O., Lim, A., Johansen, S., & Brönner, M. (2022). Crustal and thermal heterogeneities across the Fram Strait and the Svalbard Margin. *Tectonics*, *41*(10), e2022TC007302.

Eide, C. H., Klausen, T. G., Katkov, D., Suslova, A. A., & Helland-Hansen, W. (2017). Linking an early Triassic delta to antecedent topography: Source-to-sink study of the southwestern Barents Sea margin. *Geological Society of America Bulletin*, *130*(1–2), 263–283.

Eide, C. H., Müller, R., & Helland-Hansen, W. (2018). Using climate to relate water discharge and area in modern and ancient catchments. *Sedimentology*, *65*(4), 1378–1389.

Eidvin, T., Jansen, E., & Riis, F. (1993). Chronology of Tertiary fan deposits off the western Barents Sea: Implications for the uplift and erosion history of the Barents Shelf. *Marine Geology*, *112*(1), 109–131.

Eidvin, T., Riis, F., Brekke, H., & Smelror, M. (2022). A revised lithostratigraphic scheme for the Eocene to Pleistocene succession on the Norwegian continental shelf. *Norwegian Journal of Geology*, *1*, 1–132. https://doi.org/10.17850/njgsp1

Faleide, J., Myhre, A., & Eldholm, O. (1988). Early Tertiary volcanism at the western Barents Sea margin. *Geological Society, London, Special Publications*, *39*(1), 135–146.

Faleide, J. I., Bjørlykke, K., & Gabrielsen, R. H. (2015). Geology of the Norwegian continental shelf. In K. Bjørlykke (Ed.), *Petroleum geoscience: From sedimentary environments to rock physics* (pp. 603–637). Springer-Verlag.

Faleide, J. I., Tsikalas, F., Breivik, A. J., Mjelde, R., Ritzmann, O., Engen, O., Wilson, J., & Eldholm, O. (2008). Structure and evolution of the continental margin off Norway and the Barents Sea. *Episodes*, *31*(1), 82–91.

Fjeldskaar, W., & Amantov, A. (2018). Effects of glaciations on sedimentary basins. *Journal of Geodynamics*, *118*, 66–81.

Flowerdew, M. J., Fleming, E. J., Chew, D. M., Morton, A. C., Frei, D., Benedictus, A., Omma, J., Riley, T. R., Badenszki, E., & Whitehouse, M. J. (2023). The importance of Eurekan Mountains on Cenozoic sediment routing on the Western Barents shelf. *Geosciences*, *13*(3), 91.

Gac, S., Minakov, A., Shephard, G. E., Faleide, J. I., & Planke, S. (2020). Deformation analysis in the Barents Sea in relation to Paleogene transpression along the Greenland-Eurasia Plate Boundary. *Tectonics*, *39*(10), e2020TC006172.

Gaina, C., Nasuti, A., Kimbell, G. S., & Blischke, A. (2017). Break-up and seafloor spreading domains in the NE Atlantic. *Geological Society, London, Special Publications*, *447*(1), 393–417.

GEBCO. (2022). GEBCO_2022 grid.

Gervais, V., Granjeon, D., & Bouquet, S. (2023). An automatic workflow for risk analysis on spatial output properties using kriging-based surrogate models—Application to stratigraphic forward modelling. *Basin Research*, *35*, 1933–1960.

Gilmullina, A., Klausen, T. G., Doré, A. G., Rossi, V. M., Suslova, A., & Eide, C. H. (2022). Linking sediment supply variations and tectonic evolution in deep time, source-to-sink systems—The Triassic Greater Barents Sea Basin. *Bulletin*, *134*(7–8), 1760–1780.

Golovneva, L. B., Zolina, A. A., & Spicer, R. A. (2023). The early Paleocene (Danian) climate of Svalbard based on palaeobotanical data. *Papers in Palaeontology*, *9*(6), e1533.

Granjeon, D., & Joseph, P. (1999). Concepts and applications of a 3-D multiple lithology, diffusive model in stratigraphic modeling.

Green, P., & Duddy, I. (2010). Synchronous exhumation events around the Arctic including examples from Barents Sea and Alaska North Slope. *Geological Society of London, Petroleum Geology Conference Series*, *7*, 633–644.

Greenwood, D. R., Basinger, J. F., & Smith, R. Y. (2010). How wet was the Arctic Eocene rain forest? Estimates of precipitation from Paleogene Arctic macrofloras. *Geology*, *38*(1), 15–18.

Grundvåg, S.-A., Marin, D., Kairanov, B., Śliwińska, K., Nøhr-Hansen, H., Jelby, M. E., Escalona, A., & Olaussen, S. (2017). The Lower Cretaceous succession of the northwestern Barents Shelf: Onshore and offshore correlations. *Marine and Petroleum Geology*, *86*, 834–857.

Harishidayat, D., Omosanya, K. O., Johansen, S. E., Eruteya, O. E., & Niyazi, Y. (2018). Morphometric analysis of sediment conduits on a bathymetric high: Implications for palaeoenvironment and hydrocarbon prospectivity. *Basin Research*, *30*(5), 1015–1041.

Hawie, N., Covault, J. A., Dunlap, D., & Sylvester, Z. (2018). Slope-fan depositional architecture from high-resolution forward stratigraphic models. *Marine and Petroleum Geology*, *91*, 576–585.

Hawie, N., Deschamps, R., Granjeon, D., Nader, F. H., Gorini, C., Müller, C., Montadert, L., & Baudin, F. (2017). Multi-scale constraints of sediment source to sink systems in frontier basins: A forward stratigraphic modelling case study of the levant region. *Basin Research*, *29*, 418–445.

Helland-Hansen, W., & Grundvåg, S. A. (2021). The Svalbard Eocene-Oligocene (?) Central Basin succession: Sedimentation patterns and controls. *Basin Research*, *33*(1), 729–753.

Helland-Hansen, W., Sømme, T. O., Martinsen, O. J., Lunt, I., & Thurmond, J. (2016). Deciphering Earth's natural hourglasses: Perspectives on source-to-sink analysis. *Journal of Sedimentary Research*, *86*(9), 1008–1033.

Henriksen, E., Bjørnseth, H., Hals, T., Heide, T., Kiryukhina, T., Kløvjan, O., Larssen, G., Ryseth, A., Rønning, K., & Sollid, K. (2011). Uplift and erosion of the greater Barents Sea: Impact on prospectivity and petroleum systems. *Geological Society, London, Memoirs*, *35*(1), 271–281.

Henriksen, E., Ryseth, A., Larssen, G., Heide, T., Rønning, K., Sollid, K., & Stoupakova, A. (2011). Tectonostratigraphy of the greater Barents Sea: Implications for petroleum systems. *Geological Society, London, Memoirs*, *35*(1), 163–195.

Indrevær, K., Gac, S., Gabrielsen, R. H., & Faleide, J. I. (2018). Crustal-scale subsidence and uplift caused by metamorphic

phase changes in the lower crust: A model for the evolution of the Loppa High area, SW Barents Sea from late Paleozoic to present. *Journal of the Geological Society*, *175*(3), 497–508.

Jakobsson, K. (2018). A history of exploration offshore Norway: The Barents Sea. *Geological Society, London, Special Publications*, *465*(1), 219–241.

Jakobsson, M., Backman, J., Rudels, B., Nycander, J., Frank, M., Mayer, L., Jokat, W., Sangiorgi, F., O'Regan, M., & Brinkhuis, H. (2007). The early Miocene onset of a ventilated circulation regime in the Arctic Ocean. *Nature*, *447*(7147), 986–990.

Johansen, S., Ostisty, B., Fedorovsky, Y., Martirosjan, V., Christensen, O. B., Cheredeev, S., Ignatenko, E., & Margulis, L. (1993). *Hydrocarbon potential in the Barents Sea region: Play distribution and potential* (pp. 273–320). Norwegian Petroleum Society Special Publications.

Jones, S. M., Murton, B. J., Fitton, J. G., White, N. J., Maclennan, J., & Walters, R. (2014). A joint geochemical–Geophysical record of time-dependent mantle convection south of Iceland. *Earth and Planetary Science Letters*, *386*, 86–97.

Jones, S. M., & White, N. (2003). Shape and size of the starting Iceland plume swell. *Earth and Planetary Science Letters*, *216*(3), 271–282.

Jones, S. M., White, N., Clarke, B. J., Rowley, E., & Gallagher, K. (2002). Present and past influence of the Iceland Plume on sedimentation. *Geological Society, London, Special Publications*, *196*(1), 13–25.

Klausen, T. G., & Helland-Hansen, W. (2018). Methods for restoring and describing ancient clinoform surfaces. *Journal of Sedimentary Research*, *88*(2), 241–259.

Klausen, T. G., Müller, R., Slama, J., & Helland-Hansen, W. (2017). Evidence for late Triassic provenance areas and Early Jurassic sediment supply turnover in the Barents Sea Basin of northern Pangea. *Lithosphere*, *9*(1), 14–28.

Knies, J., Matthiessen, J., Vogt, C., Laberg, J. S., Hjelstuen, B. O., Smelror, M., Larsen, E., Andreassen, K., Eidvin, T., & Vorren, T. O. (2009). The Plio-Pleistocene glaciation of the Barents Sea–Svalbard region: A new model based on revised chronostratigraphy. *Quaternary Science Reviews*, *28*(9), 812–829.

Knies, J., Mattingsdal, R., Fabian, K., Grøsfjeld, K., Baranwal, S., Husum, K., De Schepper, S., Vogt, C., Andersen, N., & Matthiessen, J. (2014). Effect of early Pliocene uplift on late Pliocene cooling in the Arctic–Atlantic gateway. *Earth and Planetary Science Letters*, *387*, 132–144.

Kristensen, T. B., Rotevatn, A., Marvik, M., Henstra, G. A., Gawthorpe, R. L., & Ravnås, R. (2018). Structural evolution of sheared margin basins: The role of strain partitioning. Sørvestsnaget Basin, Norwegian Barents Sea. *Basin Research*, *30*(2), 279–301.

Ktenas, D., Henriksen, E., Meisingset, I., Nielsen, J. K., & Andreassen, K. (2017). Quantification of the magnitude of net erosion in the southwest Barents Sea using sonic velocities and compaction trends in shales and sandstones. *Marine and Petroleum Geology*, *88*, 826–844.

Ktenas, D., Nielsen, J. K., Henriksen, E., Meisingset, I., & Schenk, O. (2023). The effects of uplift and erosion on the petroleum systems in the southwestern Barents Sea: Insights from seismic data and 2D petroleum systems modelling. *Marine and Petroleum Geology*, *158*, 106535.

Laberg, J., Vorren, T., & Knutsen, S.-M. (1999). The Lofoten contourite drift off Norway. *Marine Geology*, *159*(1), 1–6.

Laberg, J. S., Andreassen, K., & Vorren, T. O. (2012). Late Cenozoic erosion of the high-latitude southwestern Barents Sea shelf revisited. *Geological Society of America Bulletin*, *124*(1–2), 77–88.

Lasabuda, A., Geissler, W. H., Laberg, J. S., Knutsen, S. M., Rydningen, T. A., & Berglar, K. (2018). Late Cenozoic erosion estimates for the northern Barents Sea: Quantifying glacial sediment input to the Arctic Ocean. *Geochemistry, Geophysics, Geosystems*, *19*(12), 4876–4903.

Lasabuda, A., Laberg, J. S., Knutsen, S.-M., & Høgseth, G. (2018). Early to middle Cenozoic paleoenvironment and erosion estimates of the southwestern Barents Sea: Insights from a regional mass-balance approach. *Marine and Petroleum Geology*, *96*, 501–521.

Lasabuda, A., Laberg, J. S., Knutsen, S.-M., & Safronova, P. (2018). Cenozoic tectonostratigraphy and pre-glacial erosion: A mass-balance study of the northwestern Barents Sea margin, Norwegian Arctic. *Journal of Geodynamics*, *119*, 149–166.

Lasabuda, A. P., Johansen, N. S., Laberg, J. S., Faleide, J. I., Senger, K., Rydningen, T. A., Patton, H., Knutsen, S.-M., & Hanssen, A. (2021). Cenozoic uplift and erosion of the Norwegian Barents Shelf–a review. *Earth-Science Reviews*, *217*, 103609.

Lasabuda, A. P. E., Hanssen, A., Laberg, J. S., Faleide, J. I., Patton, H., Abdelmalak, M. M., Rydningen, T. A., & Kjølhamar, B. E. (2023). Paleobathymetric reconstructions of the SW Barents Seaway and their implications for Atlantic-Arctic ocean circulation. *Communications Earth & Environment*, *4*, 231.

Longhitano, S. G., & Chiarella, D. (2020). Tidal straits: Basic criteria for recognizing ancient systems from the rock record. In *Regional geology and tectonics* (pp. 365–415). Elsevier.

Løtveit, I. F., Fjeldskaar, W., & Sydnes, M. (2019). Tilting and flexural stresses in basins due to glaciations—An example from the Barents Sea. *Geosciences*, *9*(11), 474.

Marín, D., Escalona, A., Grundvåg, S. A., Olaussen, S., Sandvik, S., & Śliwińska, K. K. (2018). Unravelling key controls on the rift climax to post-rift fill of marine rift basins: Insights from 3D seismic analysis of the Lower Cretaceous of the Hammerfest Basin, SW Barents Sea. *Basin Research*, *30*(4), 587–612.

Miller, K. G., Browning, J. V., Schmelz, W. J., Kopp, R. E., Mountain, G. S., & Wright, J. D. (2020). Cenozoic sea-level and cryospheric evolution from deep-sea geochemical and continental margin records. *Science Advances*, *6*(20), eaaz1346.

Miller, K. G., Kominz, M. A., Browning, J. V., Wright, J. D., Mountain, G. S., Katz, M. E., Sugarman, P. J., Cramer, B. S., Christie-Blick, N., & Pekar, S. F. (2005). The phanerozoic record of global sea-level change. *Science*, *310*(5752), 1293–1298.

Milliman, J. D., & Farnsworth, K. L. (2013). *River discharge to the coastal ocean: A global synthesis*. Cambridge University Press.

Milliman, J. D., & Meade, R. H. (1983). World-wide delivery of river sediment to the oceans. *The Journal of Geology*, *91*, 1–21.

Milliman, J. D., & Syvitski, J. P. (1992). Geomorphic/tectonic control of sediment discharge to the ocean: The importance of small mountainous rivers. *The Journal of Geology*, *100*(5), 525–544.

Müller, R. D., Zahirovic, S., Williams, S. E., Cannon, J., Seton, M., Bower, D. J., Tetley, M. G., Heine, C., Le Breton, E., & Liu, S. (2019). A global plate model including lithospheric deformation along major rifts and orogens since the Triassic. *Tectonics*, *38*(6), 1884–1907.

Nyberg, B., Helland-Hansen, W., Gawthorpe, R. L., Sandbakken, P., Eide, C. H., Sømme, T., Hadler-Jacobsen, F., & Leiknes, S. J. S. G. (2018). Revisiting morphological relationships of modern source-to-sink segments as a first-order approach to

scale ancient sedimentary systems. *Communications Earth & Environment*, *373*, 111–133.

Nyland, B., Jensen, L., Skagen, J., Skarpnes, O., & Vorren, T. (1992). Tertiary uplift and erosion in the Barents Sea: Magnitude, timing and consequences. In R. M. Larsen, H. Brekke, B. T. Larsen, & E. Talleras (Eds.), *Tectonic modelling and its implication to petroleum geology* (pp. 153–162). Elsevier.

Palerme, C., Genthon, C., Claud, C., Kay, J. E., Wood, N. B., & L'Ecuyer, T. (2017). Evaluation of current and projected Antarctic precipitation in CMIP5 models. *Climate Dynamics*, *48*, 225–239. https://doi.org/10.1007/s00382-016-3071-1

Patruno, S., Hampson, G. J., & Jackson, C. A. (2015). Quantitative characterisation of deltaic and subaqueous clinoforms. *Earth-Science Reviews*, *142*, 79–119.

Patruno, S., & Helland-Hansen, W. (2018). Clinoforms and clinoform systems: Review and dynamic classification scheme for shorelines, subaqueous deltas, shelf edges and continental margins. *Earth-Science Reviews*, *185*, 202–233.

Patton, H., Hubbard, A., Heyman, J., Alexandropoulou, N., Lasabuda, A. P., Stroeven, A., Hall, A., Winsborrow, M., Sugden, D. E., & Kleman, J. (2022). The extreme yet transient nature of glacial erosion. *Nature Communications*, *13*(1), 1–14.

Pellegrini, C., Asioli, A., Bohacs, K. M., Drexler, T. M., Feldman, H. R., Sweet, M. L., Maselli, V., Rovere, M., Gamberi, F., & Dalla Valle, G. (2018). The late Pleistocene Po River lowstand wedge in the Adriatic Sea: Controls on architecture variability and sediment partitioning. *Marine and Petroleum Geology*, *96*, 16–50.

Pellegrini, C., Patruno, S., Helland-Hansen, W., Steel, R. J., & Trincardi, F. (2020). Clinoforms and clinothems: Fundamental elements of basin infill. *Basin Research*, *32*, 187–205.

Petersen, T. G., Thomsen, T., Olaussen, S., & Stemmerik, L. (2016). Provenance shifts in an evolving Eurekan foreland basin: The tertiary Central Basin, Spitsbergen. *Journal of the Geological Society*, *173*(4), 634–648.

Piepjohn, K., von Gosen, W., & Tessensohn, F. (2016). The Eurekan deformation in the Arctic: An outline. *Journal of the Geological Society*, *173*(6), 1007–1024.

Plaza-Faverola, A., Vadakkepuliyambatta, S., Singhroha, S., Hong, W.-. L., Waghorn, K. A., Lasabuda, A. P., Ferré, B., Bünz, S., & Mienert, J. (2022). Gas hydrate related bottom-simulating reflections along the West-Svalbard Margin, Fram Strait. In J. Mienert, C. Berndt, A. M. Tréhu, A. Camerlenghi, & C. S. Liu (Eds.), *World Atlas of submarine gas hydrates in continental margins* (pp. 225–235). Springer Nature.

Plink-Björklund, P. (2020). Shallow-water deltaic clinoforms and process regime. *Basin Research*, *32*, 251–262.

Popova, S., Utescher, T., Gromyko, D., Bruch, A., & Mosbrugger, V. (2012). Palaeoclimate evolution in Siberia and the Russian Far East from the Oligocene to Pliocene–Evidence from fruit and seed floras. *Turkish Journal of Earth Sciences*, *21*(2), 315–334.

Ramberg, I. B. (2008). *The making of a land: Geology of Norway*. Geological Society of London.

Rasmussen, E., & Fjeldskaar, W. (1996). Quantification of the Pliocene-Pleistocene erosion of the Barents Sea from present-day bathymetry. *Global and Planetary Change*, *12*(1), 119–133.

Retallack, G. J. (2007). Cenozoic paleoclimate on land in North America. *The Journal of Geology*, *115*(3), 271–294.

Richardsen, G., Henriksen, E., & Vorren, T. (1991). Evolution of the Cenozoic sedimentary wedge during rifting and seafloor spreading west of the Stappen high, western Barents Sea. *Marine Geology*, *101*(1–4), 11–30.

Riis, F., & Fjeldskaar, W. (1992). On the magnitude of the Late Tertiary and Quaternary erosion and its significance for the uplift of Scandinavia and the Barents Sea. In R. M. Larsen, H. Brekke, B. T. Larsen, & E. Taleraas (Eds.), *Structural and tectonic modelling and its application to petroleum geology* (pp. 163–185). Elsevier.

Romans, B. W., Castelltort, S., Covault, J. A., Fildani, A., & Walsh, J. (2016). Environmental signal propagation in sedimentary systems across timescales. *Earth-Science Reviews*, *153*, 7–29.

Rydningen, T. A., Høgseth, G., Lasabuda, A. P. E., Laberg, J. S., Safronova, P., & Forwick, M. (2020). An early Neogene—Early Quaternary contourite drift system on the SW Barents Sea continental margin, Norwegian Arctic. *Geochemistry, Geophysics, Geosystems*, *21*(11), e2020GC009142.

Ryseth, A., Augustson, J. H., Charnock, M., Haugerud, O., Knutsen, S.-M., Midbøe, P. S., Opsal, J. G., & Sundsbø, G. (2003). Cenozoic stratigraphy and evolution of the Sørvestsnaget Basin, southwestern Barents Sea. *Norwegian Journal of Geology*, *83*(2), 107–130.

Safronova, P. A., Andreassen, K., Laberg, J. S., & Vorren, T. O. (2012). Development and post-depositional deformation of a Middle Eocene deep-water sandy depositional system in the Sørvestsnaget Basin, SW Barents Sea. *Marine and Petroleum Geology*, *36*(1), 83–99.

Safronova, P. A., Henriksen, S., Andreassen, K., Laberg, J. S., & Vorren, T. O. (2014). Evolution of shelf-margin clinoforms and deep-water fans during the middle Eocene in Sorvestsnaget Basin. *AAPG Bulletin*, *98*(3), 515–544.

Samuels, J. X., & Hopkins, S. S. (2017). The impacts of Cenozoic climate and habitat changes on small mammal diversity of North America. *Global and Planetary Change*, *149*, 36–52.

Sangster, C., Piper, D. J., Hawie, N., Pe-Piper, G., & Saint-Ange, F. (2019). Forward stratigraphic modelling of sediment pathways and depocentres in salt-influenced passive-margin basins: Lower Cretaceous, central Scotian Basin. *Basin Research*, *31*(4), 728–753.

Schubert, B. A., Jahren, A. H., Davydov, S. P., & Warny, S. (2017). The transitional climate of the late Miocene Arctic: Winter-dominated precipitation with high seasonal variability. *Geology*, *45*(5), 447–450.

Schubert, B. A., Jahren, A. H., Eberle, J. J., Sternberg, L. S., & Eberth, D. A. (2012). A summertime rainy season in the Arctic forests of the Eocene. *Geology*, *40*(6), 523–526.

Sclater, J. G., & Christie, P. A. (1980). Continental stretching: An explanation of the post-Mid-Cretaceous subsidence of the central North Sea Basin. *Journal of Geophysical Research: Solid Earth*, *85*(B7), 3711–3739.

Smelror, M., Petrov, O., Larssen, G. B., & Werner, S. (2009). *Atlas: Geological history of the Barents Sea* (p. 135). Norges Geologiske Undersøkelse.

Sømme, T. O., Helland-Hansen, W., & Granjeon, D. (2009). Impact of eustatic amplitude variations on shelf morphology, sediment dispersal, and sequence stratigraphic interpretation: Icehouse versus greenhouse systems. *Geology*, *37*(7), 587–590.

Sømme, T. O., Helland-Hansen, W., Martinsen, O. J., & Thurmond, J. B. (2009). Relationships between morphological and sedimentological parameters in source-to-sink systems: A basis for predicting semi-quantitative characteristics in subsurface systems. *Basin Research*, *21*(4), 361–387.

Sømme, T. O., Huwe, S. I., Martinsen, O. J., Sandbakken, P. T., Skogseid, J., & Valore, L. A. (2023). Stratigraphic expression of the Paleocene-Eocene thermal maximum climate event during long-lived transient uplift—An example from a shallow to deep-marine clastic system in the Norwegian Sea. *Frontiers in Earth Science*, *11*, 1082203.

Sømme, T. O., Martinsen, O. J., & Thurmond, J. B. (2009). Reconstructing morphological and depositional characteristics in subsurface sedimentary systems: An example from the Maastrichtian–Danian Ormen Lange system, Møre Basin, Norwegian Sea. *AAPG Bulletin*, *93*(10), 1347–1377.

Stow, D., Hunter, S., Wilkinson, D., & Hernández-Molina, F. (2008). The nature of contourite deposition. *Developments in Sedimentology*, *60*, 143–156.

Talwani, M., & Eldholm, O. (1977). Evolution of the Norwegian-Greenland sea. *Geological Society of America Bulletin*, *88*(7), 969–999.

Trenberth, K. E. (2011). Changes in precipitation with climate change. *Climate Research*, *47*(1–2), 123–138.

Tucker, G. E., & Slingerland, R. L. (1994). Erosional dynamics, flexural isostasy, and long-lived escarpments: A numerical modeling study. *Journal of Geophysical Research: Solid Earth*, *99*(B6), 12229–12243.

Uhl, D., Traiser, C., Griesser, U., & Denk, T. (2007). Fossil leaves as palaeoclimate proxies in the Palaeogene of Spitsbergen (Svalbard). *Acta Palaeobotanica-Krakow*, *47*(1), 89.

Vågnes, E., & Amundsen, H. E. F. (1993). Late Cenozoic uplift and volcanism on Spitsbergen: Caused by mantle convection? *Geology*, *21*(3), 251–254.

Vorren, T. O., Richardsen, G., Knutsen, S.-M., & Henriksen, E. (1991). Cenozoic erosion and sedimentation in the western Barents Sea. *Marine and Petroleum Geology*, *8*(3), 317–340.

Westerhold, T., Marwan, N., Drury, A. J., Liebrand, D., Agnini, C., Anagnostou, E., Barnet, J. S., Bohaty, S. M., De Vleeschouwer, D., & Florindo, F. (2020). An astronomically dated record of Earth's climate and its predictability over the last 66 million years. *Science*, *369*(6509), 1383–1387.

Willgoose, G., Bras, R. L., & Rodriguez-Iturbe, I. (1991). A coupled channel network growth and hillslope evolution model: 1. Theory. *Water Resources Research*, *27*(7), 1671–1684.

Zachos, J. C., & Kump, L. R. (2005). Carbon cycle feedbacks and the initiation of Antarctic glaciation in the earliest Oligocene. *Global and Planetary Change*, *47*(1), 51–66.

SUPPORTING INFORMATION

Additional supporting information can be found online in the Supporting Information section at the end of this article.